

Response of Long Valley caldera to the $M_w = 7.3$ Landers, California, Earthquake

David P. Hill, Malcolm J. S. Johnston, and John O. Langbein
U.S. Geological Survey, Menlo Park, California

Roger Bilham

Department of Geology, University of Colorado, Boulder

Abstract. Of the many sites in the western United States responding to the June 28, 1992, Landers earthquake ($M_w = 7.3$) with remotely triggered seismicity, only Long Valley caldera is monitored by both seismic and continuous deformation networks. A transient strain pulse and surge in seismicity recorded by these networks began within tens of seconds following arrival of the shear pulse from Landers. The cumulative strain and number of triggered earthquakes followed the same exponentially decaying growth rate (time constant 1.8 days) during the first 6 days following Landers. The strain transient, which was recorded on a borehole dilatometer at the west margin of the caldera and a long-base tiltmeter 20 km to the east, peaked on the sixth day at ≈ 0.25 ppm and gradually decayed over the next 15–20 days. The absence of a clear strain signal exceeding 0.4 ppm in data from the two-color geodimeter deformation lines, which span the central section of the caldera, indicates that the strain transient cannot be due solely to pressure changes in the concentrated pressure source 7 km beneath the central part of the caldera that accounts for most of the uplift of the resurgent dome since 1980. The triggered seismicity occupied the entire seismogenic volume beneath the caldera. The focal mechanisms, the frequency-magnitude distribution, and the spatial distribution of the triggered earthquakes are typical of other swarms in Long Valley caldera. The cumulative seismic moment of the triggered earthquakes through the first 2 weeks after the Landers earthquake corresponds to a single $M = 3.8$ earthquake, which is too small by nearly 2 orders of magnitude to account for the 0.25-ppm peak amplitude of the observed strain transients. Evidently, the strain transient represents the dominant response mode, which precludes direct triggering of local earthquakes by the large dynamic stresses from Landers as the dominant process. Conditionally viable models for the triggering process beneath the caldera include (1) the transient pressurization of magma bodies beneath the resurgent dome and Mammoth Mountain by the advective overpressure of rising bubbles, (2) a surge in fluid pressure within the seismogenic zone due to upward cascading failure of isolated compartments containing superhydrostatic pore fluids, (3) relaxation (fluidization) of a partially crystallized magma body or dike intrusion in the deep crustal roots of Long Valley magmatic system, or (4) aseismic slip on midcrustal faults. Either the deep, relaxing-magma body or lower crustal dike intrusion satisfy all the strain observations with a single deformation source. The latter model admits the possibility that large, regional earthquakes can trigger the episodic recharge of the deep roots of crustal magmatic systems.

Introduction

The $M_w = 7.3$ Landers, California, earthquake of June 28, 1992, triggered an abrupt increase in local earthquake activity at 15 widely scattered sites across much of the western United States [Hill *et al.*, 1993; Anderson *et al.*, 1994; Bodin and Gomberg, 1994; Gomberg and Bodin, 1994; Roquemore and Simila, 1994]. This unambiguous evidence for a causal link between the occurrence of a large earthquake and increased seismicity at sites separated from the mainshock rupture zone by multiple source dimensions has

Copyright 1995 by the American Geophysical Union.

Paper number 95JB00860.
0148-0227/95/95JB-00860\$05.00

forced a reassessment of the physical behavior of the Earth's crust and consideration of possible nonlinear interactions with transient and static components of the stress field produced by a large earthquake.

Of the 15 recognized sites with seismicity remotely triggered by the Landers mainshock, only Long Valley caldera in eastern California (LV in Figure 1) is monitored by both a dense seismic network and continuous deformation-monitoring instrumentation. We use this unique data set to study the response of Long Valley caldera to the Landers earthquake for clues to the processes driving the remotely triggered activity. Following a short summary of the remote seismicity triggered by the Landers earthquake and the setting of Long Valley caldera, we describe the properties of

the triggered seismicity and the transient strain pulse detected by the deformation-monitoring instrumentation in the caldera. We focus the remainder of the paper on implications of these observations for macroscopic models of the triggering process in terms of local dislocation sources capable of producing both the observed surge in seismicity and deformation transients. In this paper, we do not explore the next lower level of explanation (microscopic models) involving quantitative relations between stress/strain intensities and durations from the Landers mainshock and critical thresholds in nonlinear constitutive relations (see, for example, J. Gomberg and S. Davis, *Stress/strain changes and seismicity at The Geysers, California*, submitted to *Journal of Geophysical Research*, 1994).

Background

Landers Mainshock and Triggered Seismicity

Long Valley caldera is located just over 400 km north-northwest of the Landers mainshock epicenter (Figure 1), and it lies midway along the eastern California shear zone and the coincident Sierra Nevada–Great Basin boundary zone seismic belt. As indicated in Figure 1, most of the seismicity triggered by the Landers mainshock was concentrated within this eastern California shear zone and its northward extension toward the southernmost Cascade volcanoes, Lassen Peak and Mount Shasta [Hill et al., 1993]. The Landers mainshock rupture propagated in a unilateral direction to the north-northwest focusing most of the radiated seismic energy along the eastern California shear zone [Sieh et al., 1993; Hill et al., 1993; Kanamori et al., 1992]. Static stress changes produced by the mainshock, which decrease with distance as $1/r^3$, dropped below daily tidal stress fluctuations (≈ 0.01 bar) beyond about 200 km from the rupture surface. Peak dynamic stresses, however, which propagated with the shear wave and the crustal Love and Rayleigh waves with periods from 10 to 20 s, were approximately 3 bars in the vicinity of Long Valley caldera over 400 km north of the Landers epicenter [see Hill et al., 1993].

Setting and Recent Activity of Long Valley Caldera

Long Valley caldera has produced numerous volcanic eruptions since the caldera-forming eruption 730,000 years ago, the most recent of which vented from the Inyo Domes some 550 years ago [Bailey et al., 1976]. Current unrest within the caldera began in 1980 and includes episodic earthquake swarms accompanied by steady inflation of the resurgent dome [Hill et al., 1985; Bailey and Hill, 1990]. Earthquake swarm activity is largely confined to the southern part of the caldera extending beneath Mammoth Mountain at the southwestern margin of the caldera and into the Sierra Nevada block to the south. Maximum focal depths vary from 12 to 15 km beneath the Sierra Nevada block to less than 6 km beneath the resurgent dome in the central part of the caldera [Hill, 1993]. This seismicity has maintained a relatively stable spatial distribution since the early 1980s and is typified by the 1988–1992 distribution illustrated in Figure 2. Most of the 60-cm uplift of the resurgent dome that has accumulated since 1979–1980 can be modeled by pressure increase in a concentrated volume (a Mogi source) located 7–8 km beneath the central part of the resurgent dome (Figure 2). The volume increase at the inflation source

consistent with the deformation data through 1993 is approximately 0.3 km^3 .

Monitoring Networks

The seismic and deformation monitoring networks installed in Long Valley caldera in the early 1980s to track the recently increased activity [Hill, 1984; Hill et al., 1991] are illustrated in Figure 3. The seismic network includes 18 stations within and immediately adjacent to the caldera and an additional 17 stations within 50 km of the caldera. The detection threshold for this network within the caldera is approximately $M = 0.5$, and the hypocentral locations of well-recorded (generally, $M > 1.0$) events within the caldera are good to within 1 km horizontally and 2 km vertically. In what follows, we use events of all magnitudes listed in the archive file with reported horizontal errors ≤ 1 km and vertical errors ≤ 2 km.

Telemetered deformation-monitoring instruments include two borehole dilatometers (Sacks-Evertson volumetric strain meters POPA and PLV1), seven shallow (2–10 m deep) borehole tiltmeters [Mortensen and Hopkins, 1987], and an L-shaped, long-base (0.5 km) Michelson interferometer tiltmeter, LBT [Behr et al., 1989]. Both the POPA borehole dilatometer and the Michelson long-base tiltmeter (LBT) record clear Earth tides. The dilatometer is capable of resolving strain changes of 0.005 ppm spanning periods of a few hours to a few days and 0.05 ppm over periods of months [Johnston et al., 1994]. Because of poor coupling, however, the borehole dilatometer PLV1 in the west moat of the caldera provides reliable data only for strain changes with periods less than a few hours. The tiltmeter (LBT) has a resolution of $5 \times 10^{-4} \mu\text{rad}$ and is referred to the base of three boreholes with a mean depth of 19 m. The network of shallow borehole tiltmeters is intended to track large, rapid deformation episodes typical of volcanic crises; it is capable of resolving tilts greater than 5 to 10 ppm over periods of days to weeks.

Water levels in seven wells within the caldera (see Figure 3) are sampled at intervals from 30 s to 15 min as part of an effort to monitor the hydrologic and geochemical regime in Long Valley caldera [Farrar et al., 1985]. The open intervals in most of these wells range from 150 to 200 m below the surface. The open intervals in wells RDO-8 and LKT are 338 to 341 m and 152 to 1067 m, respectively [see Roeloffs et al., 1995].

The lengths of seven baselines extending from the bench mark CASA on the resurgent dome (Figure 3) are measured several times a week using a two-color geodimeter [Langbein, 1989] to track horizontal deformation across the caldera. These data resolve strain changes in excess of 0.4 ppm at the 95% confidence level over periods of days to years.

Triggered Response of Long Valley Caldera

Long Valley caldera responded to the Landers mainshock with a surge in seismicity and a transient strain pulse that began while the *S* wave coda and crustal surface waves from the mainshock were still passing through the caldera. Peak dynamic strains from the mainshock were of the order of 10 ppm in the vicinity of the caldera, with corresponding peak dynamic stresses of the order of 3 bars [Hill et al., 1993] (also see Gomberg and Bodin [1994]): they accompanied the

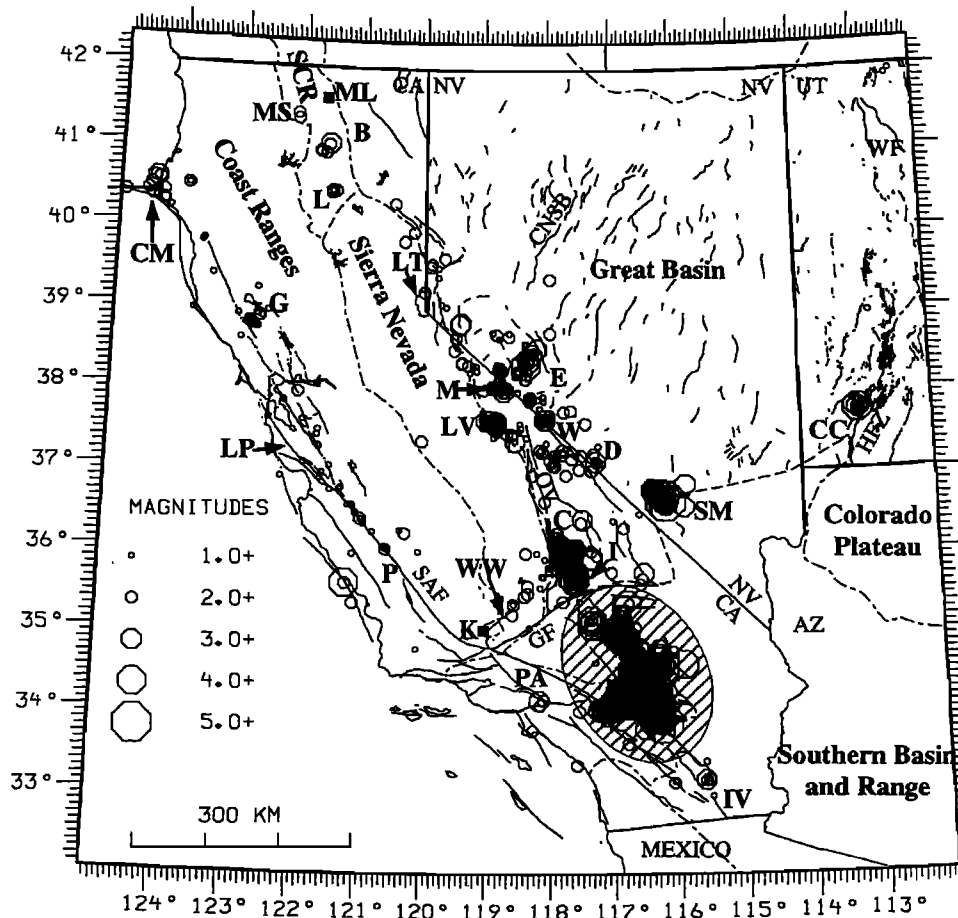


Figure 1. Map showing earthquake activity in California, Nevada, and western Utah in the first 10 days following the Landers earthquake. Major physiographic provinces are outlined by dashed lines. Faults with Quaternary slip are shown as solid lines. Shaded ellipse indicates approximate extent of Landers aftershock zone. Abbreviations are AZ, Arizona; B, Burney; C, Coso Hot Springs; CA, California; CC, Cedar City, CM, epicenter of the 1992 Petrolia (Cape Mendocino) $M = 7.2$ earthquake; CNSB, central Nevada seismic belt; D, Death Valley; E, Excelsior Mountains; G, The Geysers geothermal area; HFZ, Hurricane fault zone; I, Indian Wells Valley; IV, Imperial Valley; K, epicenter of 1952 Kern County $M = 7.5$ earthquake; LP, epicenter of the 1989 Loma Prieta $M = 6.9$ earthquake; L, Lassen Peak; LV, Long Valley caldera; LT, Lake Tahoe; M, Mono basin; ML, Medicine Lake caldera; MS, Mount Shasta; NV, Nevada; O, Owens Valley; P, Parkfield; PA, Pasadena; SAF, San Andreas fault; SCR, Southern Cascade Range; SM, Little Skull Mountain; UT, Utah; W, White Mountains; WF, Wasatch fault; WW, White Wolf fault. From Hill *et al.* [1993] (reprinted from *Science* with permission).

crustal Rayleigh and Love wave group of surface waves, which have periods ranging from 10 to 20 s and wavelengths of crustal dimensions (15–50 km). The observed coseismic static dilatational strain in the vicinity of the caldera from the Landers mainshock was a $0.006 \mu\text{strain}$ ($\approx 0.003 \text{ bar}$) compressional step [Hill *et al.*, 1993], seemingly too small (10^{-3} smaller than peak dynamic strains and 10^{-1} smaller than daily tidal strains) to be important in the triggering process.

Seismicity

The pronounced surge in seismicity rate within Long Valley caldera immediately following the Landers mainshock stands out clearly in plots of earthquake moment and cumulative number with time (Figure 4). Michael [1992] showed that the first earthquakes triggered within the caldera began approximately 40 s after arrival of the Landers

S wave, or about 3 min after the Landers origin time ($dT = 3 \text{ min}$, where we use dT to designate time lapsed after the origin time of the Landers mainshock) and during passage of the S wave coda.

The triggered activity began beneath the southwestern margin of the resurgent dome at a depth of 6–8 km (Figure 5d). This same volume has produced the most frequent and intense swarm activity within the caldera since 1980. The initial activity in this volume included a $M = 2.2$ event at $dT = 16 \text{ min}$ and a $M = 2.6$ event at $dT = 32 \text{ min}$ at depths of 7 and 8 km, respectively. By $dT = 34 \text{ min}$, triggered seismicity began near the southeast margin of the resurgent dome some 6 km east of the initial activity. As the space-time seismicity plots in Figure 5 indicate, much of the southern part of the caldera became activated within 2 hours of the Landers mainshock with no evidence for coherent

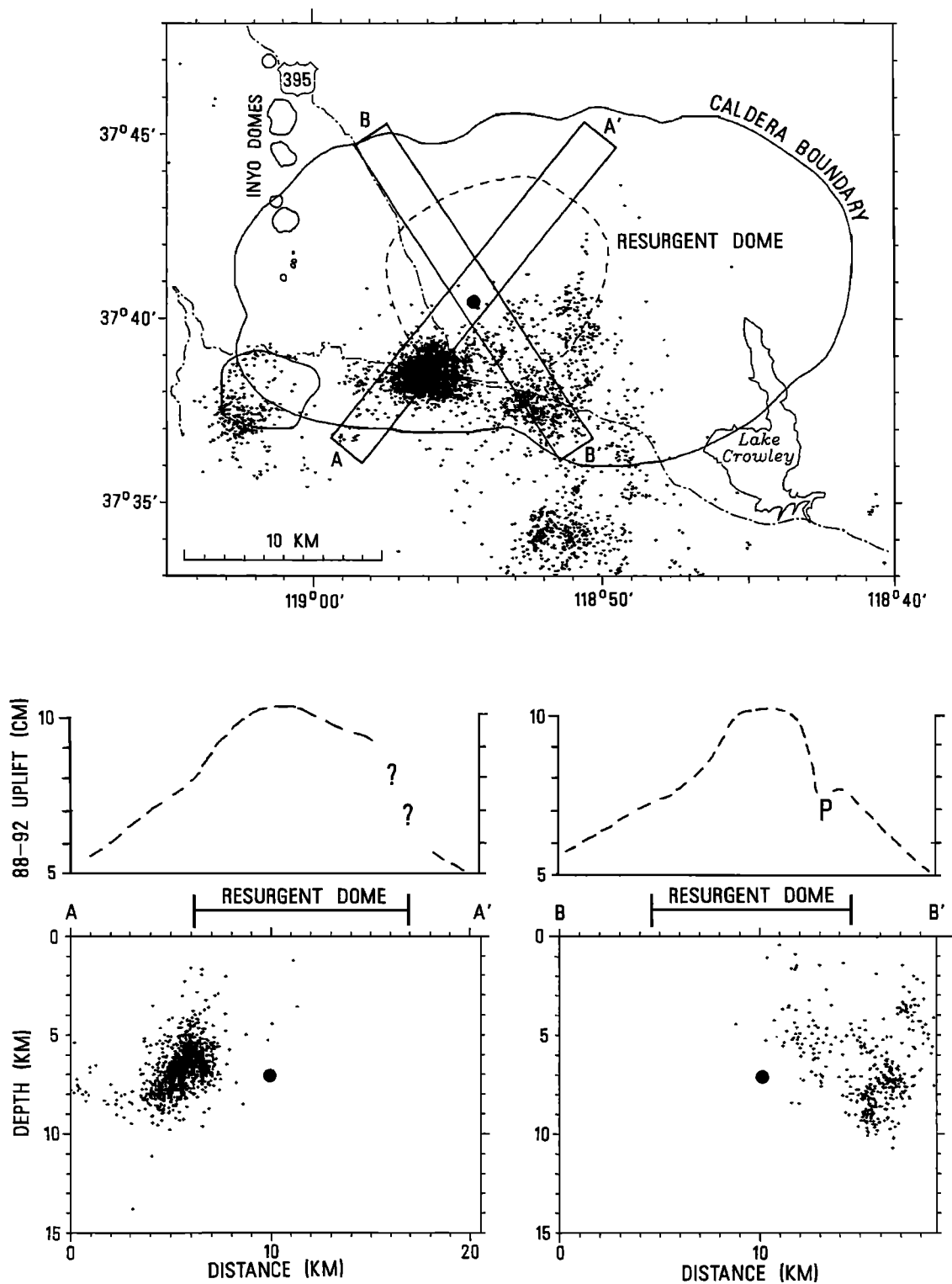


Figure 2. Epicentral locations of $M \geq 1.5$ earthquakes in Long Valley caldera from 1988 through 1992. Sections AA' and BB' show approximate elevation change across resurgent dome from 1988 to 1992 [Langbein *et al.*, 1995] and seismicity depth sections. Solid circle is location of inflation source that accounts for uplift of the resurgent dome [Langbein *et al.*, 1993]. P indicates local depression associated with power production from a geothermal energy plant.

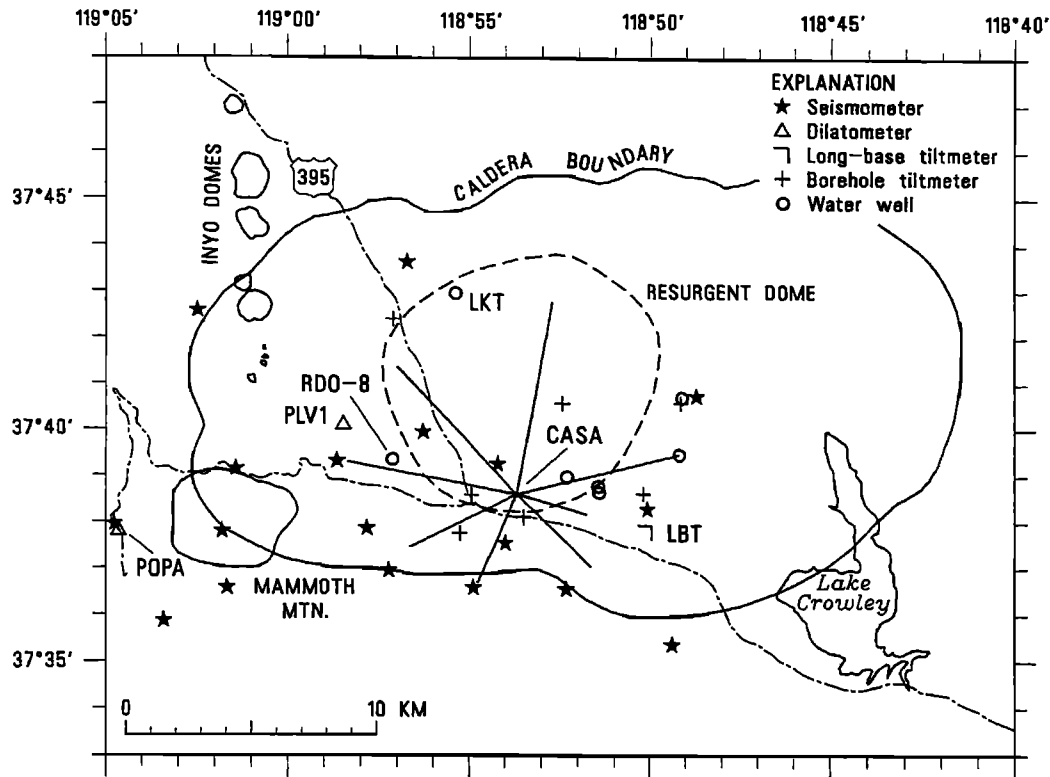


Figure 3. Map showing principal monitoring networks in Long Valley caldera. Instrument types listed in explanation. Straight lines are baselines most frequently measured by the two-color geodimeter from the bench mark CASA.

migration from the site of initial activity. In contrast, most earthquake swarm activity in the caldera occurs in relatively tight spatial clusters within the seismogenic zone with one or, less commonly, two clusters active at a time. Only the largest swarms (such as the January 1983 swarm with two $M > 5$ events) have involved activity throughout the seismogenic southern half of the caldera. Comparison with Figure 2 emphasizes that the triggered seismicity occupied most of the recently active seismogenic crust beneath the caldera. The seismogenic crust beneath Mammoth Mountain, however, which produced a 6-month-long earthquake swarm in 1989 [Hill *et al.*, 1991] but has since been relatively quiet, did not respond to the Landers earthquake.

Over the next 17 hours, seismicity gradually became concentrated in a diffuse north trending band south of the eastern margin of the resurgent dome (between longitude $118^{\circ}50'$ and $51'W$). A $M = 3.7$ earthquake along the southern extension of this zone 3 km south of the caldera occurred at 0537 UT ($dT = 17$ hours, 32 min) the next day (June 29). This was the largest of two $M > 3$ events in the triggered sequence; the other ($M = 3.4$) occurred 2.4 hours later (0758 UT; $dT = 20$ hours, 00 min) at a depth of 7 km beneath the town of Mammoth Lakes (the westernmost event plotted in Figures 5 and 6). Note that the $M = 3.7$ event appears to coincide with renewed activity throughout the southern part of the caldera (secondary triggering?). Activity throughout the area gradually returned to background seismicity rates of five to six events per day over the next 6 to 7 days (see Figures 4 and 8).

The cumulative moment of the surge in triggered seismicity is 2.5×10^{22} dyn/cm, or the equivalent of a single $M =$

3.8 earthquake (Figure 4). The dominant contributions to the cumulative seismic moment come from the $M = 3.7$ and $M = 3.4$ events at 17 hours 39 min and 20 hours 00 min after Landers, respectively (see Figure 6).

Focal mechanisms for earthquakes occurring in the south moat of the caldera typically show a mix of strike-slip and normal solutions with subhorizontal T axes oriented in a northeast-southwest direction [Savage and Cockerham, 1983; Langbein *et al.*, 1993]. Focal mechanisms for caldera earthquakes triggered by the Landers mainshock show no significant deviation from this pattern. In particular, as illustrated in Figure 6, $M > 2$ earthquakes occurring during the first 24 hours following the Landers mainshock have focal mechanisms that range from oblique-normal to nearly pure strike-slip with T axes in the northeast-southwest quadrants. Two of the events in the west moat ($dT = 34$ min and $dT = 20$ hours 00 min) have subhorizontal nodal planes with the complementary, vertical planes striking in an east-west direction.

These focal mechanisms are consistent with recognized structural relations within the caldera. Those mechanisms with a dominant dip-slip component are associated with normal slip on northwest striking faults that cut the resurgent dome [Bailey, 1989], and those with a dominant strike-slip component involve right-lateral slip on near-vertical, easterly striking faults beneath the south moat. This south moat fault system, which has no surface expression, likely represents a reactivated section of the ring-fracture fault system formed during caldera collapse [Savage and Cockerham, 1983]. The two earthquakes with subhorizontal nodal planes involve either dip slip on a near-vertical fault with the north

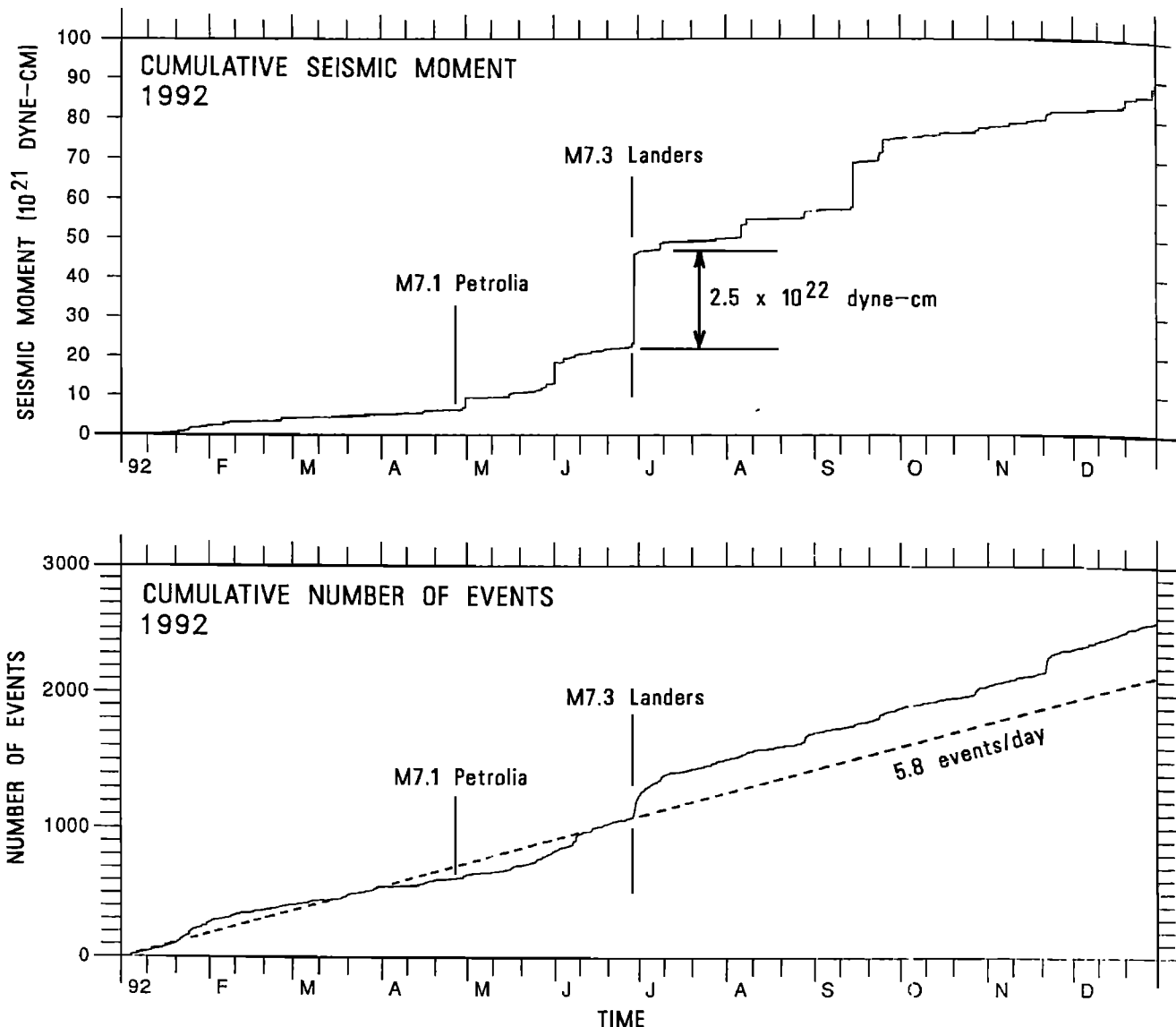


Figure 4. (top) Cumulative seismic moment for earthquakes occurring within the area of Figure 3 during 1992. Double arrow indicates cumulative seismic moment for seismicity triggered by the Landers earthquake. (bottom) Cumulative number of earthquakes during 1992 for the same area. Dashed line indicates average seismicity rate of 5.8 events/d. This includes all archived earthquakes for which the estimated horizontal and vertical location errors are less than 1 km and 2 km, respectively. Times of the $M = 7.1$ Petrolia (Cape Mendocino) and $M = 7.3$ Landers earthquakes are indicated by vertical lines.

(caldera) side up or subhorizontal slip on a surface slightly over 7 km deep with the top block moving north (toward the resurgent dome) with respect to the deeper block. The first interpretation is consistent with geodetic data, which show uplift of the resurgent dome driven by a pressure source at a depth of 7 km. The focal mechanism for the $M = 3.7$ event just south of the caldera ($dT = 17$ hours 39 min) represents left-lateral slip along a north striking fault plane consistent with most other earthquakes in the Sierra Nevada block south of the caldera [Lide and Ryall, 1985].

The frequency-magnitude distribution of the triggered earthquakes fits the Gutenberg-Richter relation with a b value of 0.96 ± 0.06 for events above a nominal completeness threshold of $M = 1.0$, and the rate of decline in activity with time follows Omori's law with $p = 1.2$ and $c = 0.75$ (see Figure 7). These values are typical of most earthquake

sequences [Kisslinger and Jones, 1991]. In essence, then, the surge in triggered seismicity in Long Valley caldera differs from on-going seismicity only in that it involved an abrupt rate increase throughout the recently active seismogenic crust beneath the caldera. Evidently, the seismicity triggered in the vicinity of Long Valley caldera was confined to crustal volumes that were near the brittle failure threshold prior to the Landers earthquake. The crust beneath Mammoth Mountain, for example, which has been largely aseismic since the 1989 swarm, did not respond to the Landers earthquake with triggered seismicity even though it did respond with a compressional strain transient, as described in the next section.

The surge in triggered seismicity occurred against a background seismicity rate of 5.8 events/d that persisted for 15 days prior to and several month after the Landers event

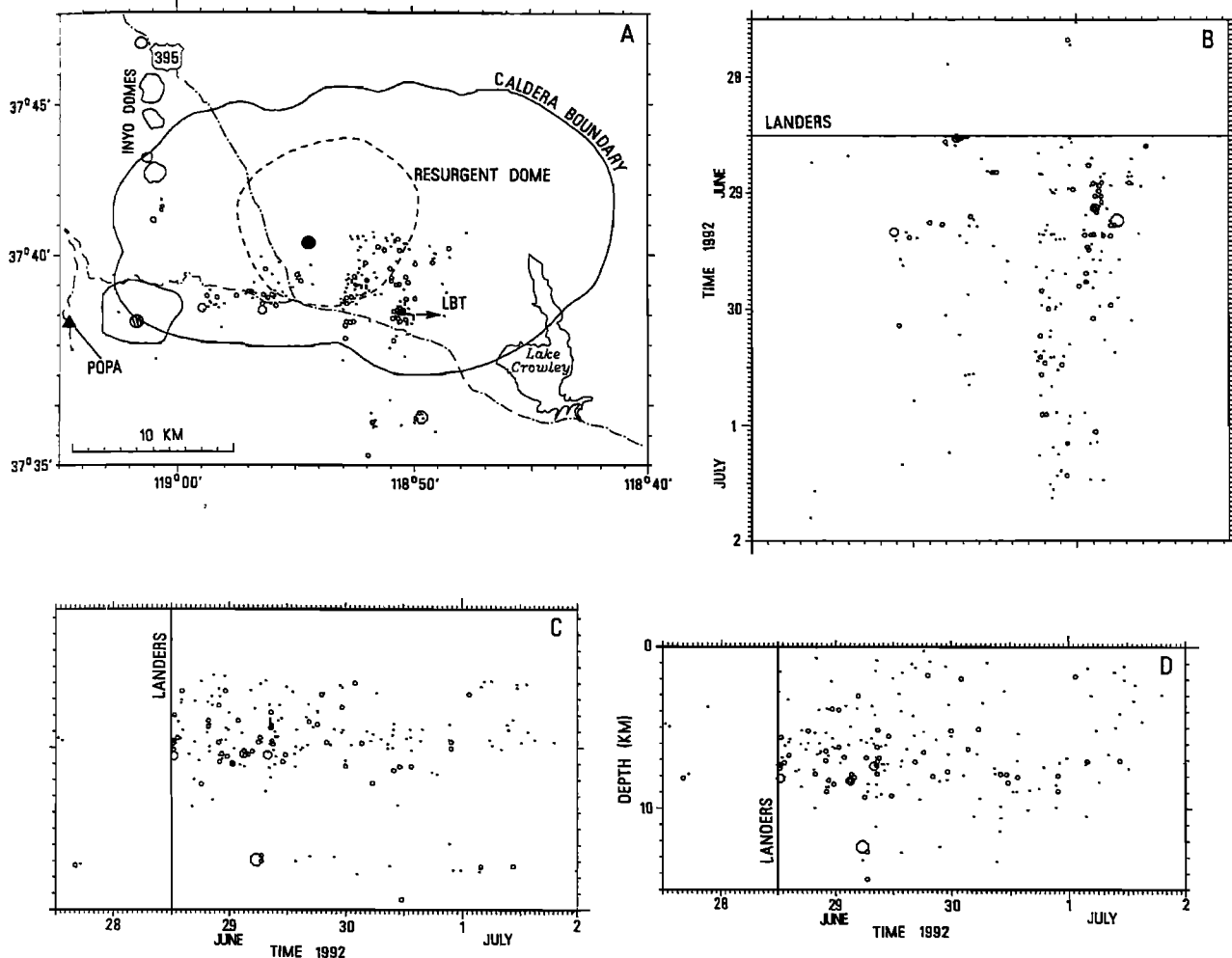


Figure 5. Space-time evolution of seismicity in Long Valley caldera triggered by the $M = 7.3$ Landers, California, earthquake. Plots show seismicity from June 28 through July 1, 1992. Circle size is proportional to earthquake magnitude scaled in four steps: $M = 0.0-1.4$, $M = 1.5-2.4$, $M = 2.5-3.5$, $M > 3.5$. (a) Epicenter map; solid triangle indicates location of POPA dilatometer; location of long-base tiltmeter (LBT). The solid circle is location of the 7-km-deep inflation center (Mogi source) beneath the resurgent dome; the shaded circle is location of the shallow Mogi source beneath Mammoth Mountain (see Figures 12a and 12b, respectively). (b) Space-time plot along east-west section; solid line indicates 1159 UT origin time of Landers mainshock on June 28. (c) Space-time plot along north-south section. (d) Depth-time plot of all events in Figure 5a.

(Figure 4). Apparently, the triggered surge involves activity in addition to a stable background rate and not simply an advance in the timing of earthquakes driven by a steady, long-term loading rate. The temporal form of the triggered sequence with the background rate removed follows the exponential aftershock decay law proposed by *Mogi* [1962] (also see *Kisslinger* [1993]), or $N(t) = (1 - e^{-at})$, with the time constant, $1/a = 1.8$ days. This exponential form for the temporal evolution of the triggered sequence will be of interest below when we compare the surge in seismicity with the triggered strain transients.

Strain and Tilt

Data documenting the strain response of Long Valley caldera to the Landers mainshock are summarized in Figure 8 modified from *Johnston et al.* [1995]. Both the borehole dilatometer POPA, located at the western base of Mammoth Mountain, and the long-base tiltmeter LBT, located near the

southeastern margin of the resurgent dome within the caldera (see Figures 3 and 5) recorded a transient strain pulse that began as the dynamic waves passed through the caldera. The sense of the dilatational strain transient at POPA was contraction (a volume decrease, or negative dilation), and the sense of the tilt transient at LBT was down to the east (taken to be positive). On both instruments the transient pulse grew to a peak amplitude of just over 0.2 ppm through the first 6 days and then gradually decayed over the next 10–30 days. Frequent measurement of seven geodetic baselines spanning the central section of the caldera (see Figure 3) during this period showed no horizontal strains above the 0.4 ppm resolution of this network accompanying the Landers earthquake [*Johnston et al.*, 1995].

The strain transient was too small to be detected by either the network of shallow borehole tiltmeters, which can resolve tilt changes greater than 5–10 ppm/week, or the PLV1 borehole dilatometer, which provides reliable information

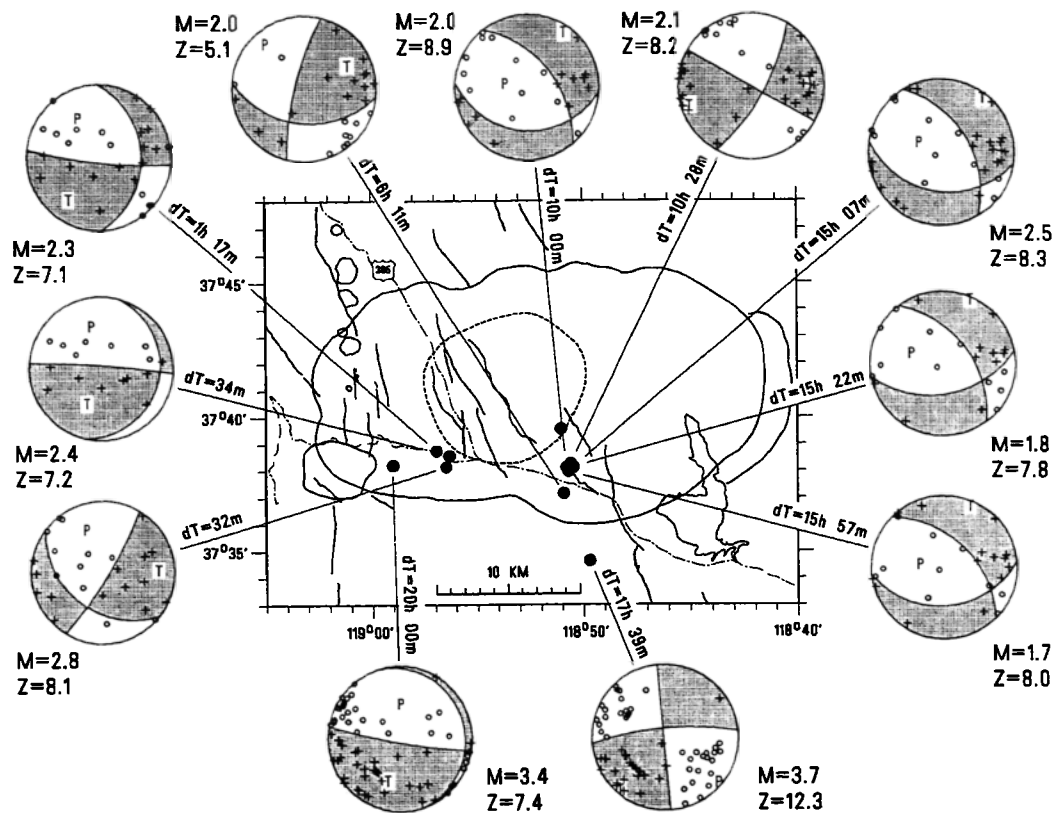


Figure 6. Fault plane solutions for $M \geq 2$ earthquakes triggered by the Landers mainshock; lower hemisphere projections. Compressional quadrants are shaded; P and T are compressional and extensional axes, respectively; dT is time after Landers origin time increasing clockwise from left; M is magnitude and Z is focal depth in kilometers.

only on strain changes that occur over periods of an hour or less.

Water Well Data

Roeloffs *et al.* [1995] summarize the hydrologic effects produced by the Landers earthquake in California and southern Oregon, including the response of the water wells

monitored in Long Valley caldera (Figure 3). They found that the water levels in all of the wells responded to the passing dynamic waves from the Landers mainshock with amplitudes ranging from 3 cm to 1.8 m (because the sample interval in most of these well is 15 to 30 min, however, these records are badly aliased with respect to the 10- to 20-s period of the peak elastic strains associated with waves from

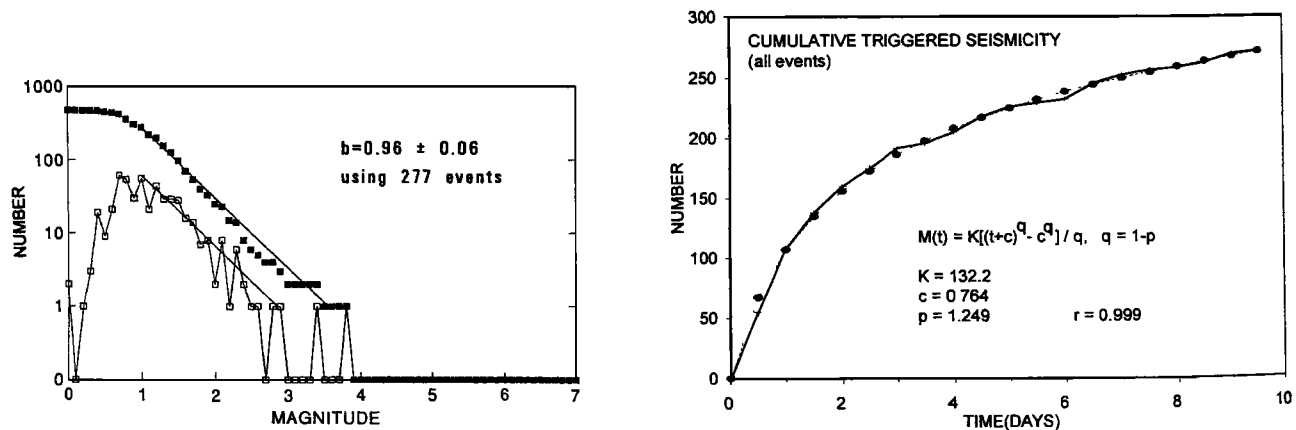


Figure 7. (left) Frequency-magnitude distribution of triggered earthquakes. Solid squares indicate total number of earthquakes equal to or smaller than a specified magnitude; open squares indicate number of earthquakes in each 0.1 magnitude interval. (right) Fit of modified Omori's law to cumulative number of triggered earthquakes with time; r is Parson's correlation coefficient.

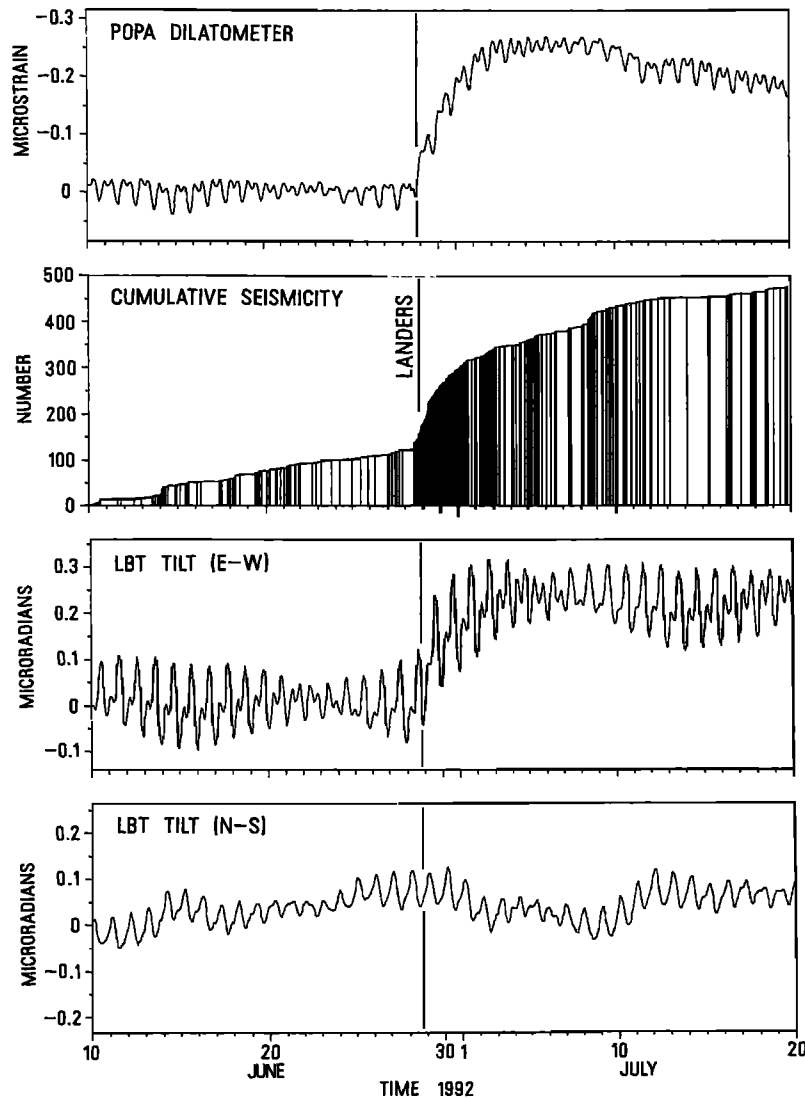


Figure 8. Triggered strain transient and seismicity for the time interval June 10 through July 19. Vertical line is time of the Landers mainshock (1157 UT, June 28). (top) POPA dilatational strain with annual trend removed (see Figure 10). Negative strain (contraction) is plotted upward to facilitate comparison with cumulative seismicity. (middle) Cumulative number of earthquakes from Figure 4. (bottom) East-west and north-south components of LBT tilt (positive is tilt down to the east and north, respectively). Modified from Johnston *et al.* [1995].

the Landers mainshock). With the exception of the RDO-8 well in the west moat of the caldera, the observed water levels in all of the wells returned to within a centimeter or so of normal within minutes to a few hours after the Landers earthquake. Because the strain sensitivity of the water wells is typically of the order of 0.01 to 0.03 cm of water level change per nanostrain, some of the Long Valley wells may reflect strain changes as large as 0.1 to 0.2 ppm (S. Rojstaczer, personal communication, 1994). In the case of RDO-8, a 12-cm drop in water level persisted for at least 2 days after the Landers event (Roeloffs *et al.* [1995] report a similar long-term drop in water level in a well near Grants Pass, Oregon). Unfortunately, the pressure transducer in the Lookout Mountain well (LKT) located in the central part of the resurgent dome failed as the Landers surface waves passed through the caldera.

Temporal Form of the Strain Transient

Figure 9 shows the complete strain history recorded by the POPA dilatometer for 1992. The compressional strain transient triggered by the Landers mainshock stands out clearly on a broad annual excursion that bottoms in mid-June. Annual fluctuations in dilatational strain at POPA routinely reach maximum compressional strain in midsummer apparently in relation to annual snow load and spring runoff cycles. The specific shape for the tail of the residual strain transient, however, depends on rather arbitrary choices for the fit to the annual trend through the strain transient and beyond. For the cubic spline fit shown in Figure 9, the strain transient returns to background by late August with no long-term offset. Other reasonable choices admit the possibility of a more extended tail and a long-term offset on one

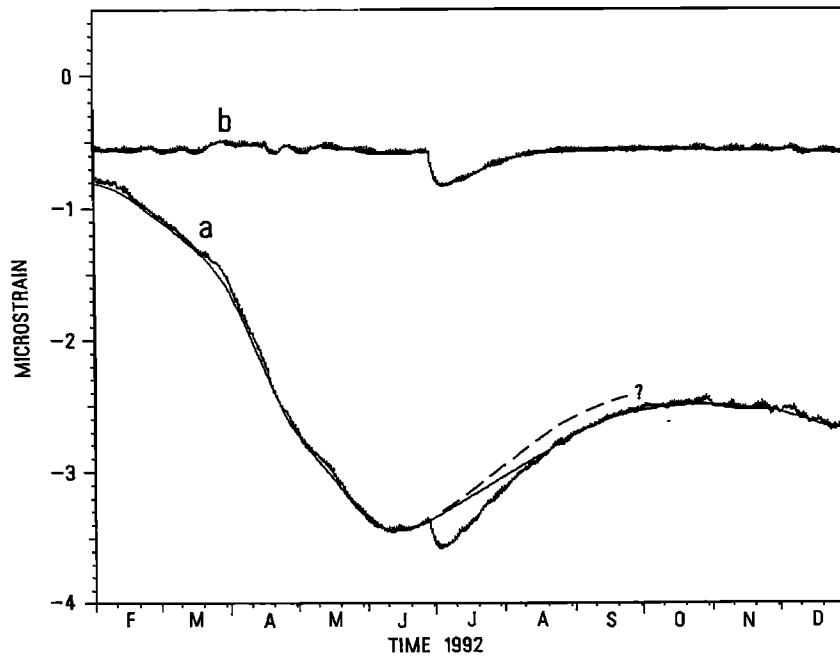


Figure 9. Dilatational strain recorded by the POPA dilatometer for 1992. Curve a is total strain. Thin line is cubic spline fit to annual trend. Dashed line suggests an alternate choice for the annual trend that would result in a more gradual decay in the residual transient with the possibility of a long-term offset. Residual strain (curve b) is the difference between the total strain (curve a) and the cubic spline fit to the annual trend.

hand (dashed line in Figure 9) or a more abbreviated tail with a small, oscillatory overshoot on the other (not shown). Similar comments apply to the tilt transient, although because of a higher background noise level at periods of days to weeks and failure of a temperature compensation probe on July 20 (22 days after Landers), the form and duration of the tail to the tilt transient are less certain. In any case, both the tilt and dilatational strain transient show evidence for at least a partial reversal in sense after 6 days and a gradual decay over the next 10–30 days.

Both the residual strain transient at POPA (curve b in Figure 9) and the tilt transient at LBT are fit remarkably well through the first 15–20 days after Landers by the difference between two decaying exponentials, or

$$\text{Ex}(t) = C(e^{-pt} - e^{-qt}) \quad (1)$$

where $|C| \approx 0.38$ ppm and the two time constants, $1/p$ and $1/q$, are 22.2 and 2.8 days, respectively (Figure 10). A second function that provides an acceptable fit to the residual transient within the uncertainties of the annual trend is

$$\text{Er}(t) = A[\text{erf}(t_c/t)^{1/2} - e^{-qt}] \quad (2)$$

where $\text{erf}(x)$ is an error function, $|A| \approx 0.36$ ppm, and $t_c \approx 4.5$ days is a characteristic diffusion time. Physically, decaying exponentials are characteristic of relaxation processes, and error functions are characteristic of diffusion processes. Equation (1) thus represents competition between two relaxation processes activated at $t = 0$; the short time constant controls the growth of the strain transient and the long time constant controls its decay. Similarly, equation (2) represents competition between a relaxation process and a diffusion process both activated at $t = 0$. Here, the relaxation

process with a short time constant controls the growth of the strain transient and the diffusion process with the longer time constant controlling its decay. Recognizing that the crust beneath Long Valley caldera includes both magma and a hydrothermal system, it is natural to anticipate that the form of the strain transients reflects some combination of viscoelastic relaxation processes perhaps coupled with a poroelastic response to fluid diffusion.

Relation Between Triggered Seismicity and the Strain Transient

As is evident in Figure 11, the growth phase of the cumulative number of triggered earthquakes and the tilt and strain transients have similar time histories through the first 6 days after Landers. Indeed, with the background seismicity rate of 5.8 events/d (see Figure 4) removed from the cumulative number of triggered earthquakes, all the time series closely follow a relaxation function of the form

$$f(t) = C(1 - e^{-at}) \quad (3)$$

with the time constant, $1/a \approx 1.8$ days common to all three processes. Both the strain and tilt transients peaked at $t \approx 6$ days, as the seismicity surge decayed to the pre-Landers rate.

Peak amplitudes at POPA and LBT, however, are much larger than can be accounted for by brittle slip associated with the triggered earthquakes based on calculations using Okada's [1992] solutions for dislocations in an elastic half-space. Surface strains and tilts due to a $M = 3.8$ earthquake (moment equivalent to the cumulative seismic moment of the triggered sequence; see Figure 4) located midway between POPA and LBT and at a depth of 7 km, for example, are less

than 0.02 ppm. Similarly, dilatational strain at POPA calculated for the $M = 3.4$ event at the western margin of the triggered sequence is less than 0.01 ppm. Maximum surface tilts calculated for the sequence of $M = 1.7-2.5$ events clustered at a depth of 8 km just 1 km west of LBT are only $0.003 \mu\text{rad}$.

Thus it appears that the strain transient is the dominant response of the caldera to the Landers earthquake with the surge in seismic activity representing a secondary process. Indeed, the relation between the loading phase of the strain transient (the first 6 days) and the triggered seismicity is reminiscent of laboratory experiments, in which observed acoustic emission rates track applied loading rates and anelastic deformation of the rock sample due to brittle slip on microcracks that produce acoustic emissions [Lockner, 1993].

Similar strain transients have not accompanied previous caldera earthquake swarms with comparable cumulative seismic moments ($\sum M_0 < 1 \times 10^{23}$ dyn cm). Thus the close temporal correlation between cumulative seismicity and strain transients illustrated in Figure 11 appears to be a unique aspect of the triggered response of the caldera to the Landers earthquake. The cumulative seismicity and strain in the caldera, however, do correlate over much longer time-scales as Langbein *et al.* [1993] demonstrate for the episode

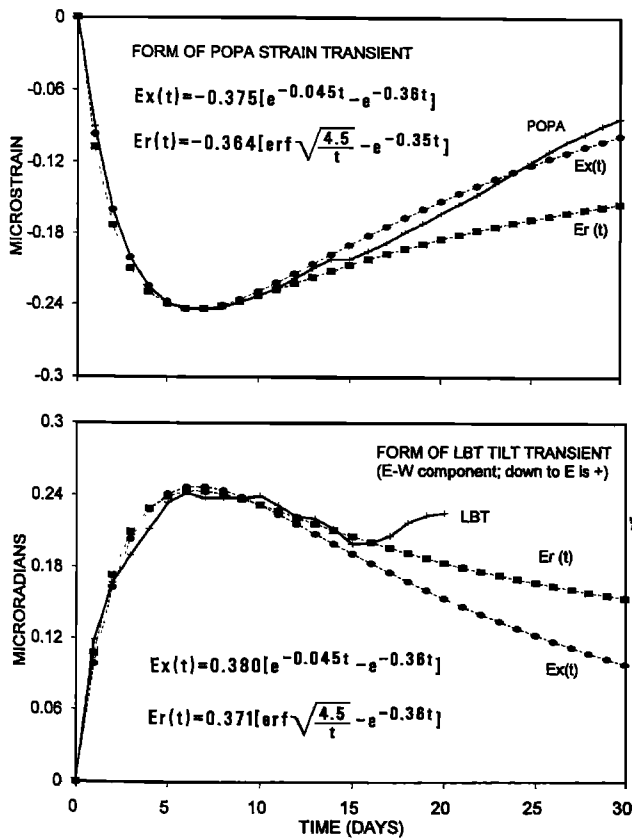


Figure 10. Functional form of the strain transient through the first 30 days after the Lander mainshock comparing fit by equations (1) and (2). (top) Residual dilatational strain at POPA (curve b in Figure 9) with tides and annual trend removed. (bottom) East component of tilt at LBT with tides removed. $Ex(t)$ and $Er(t)$ are equations (1) and (2), respectively.

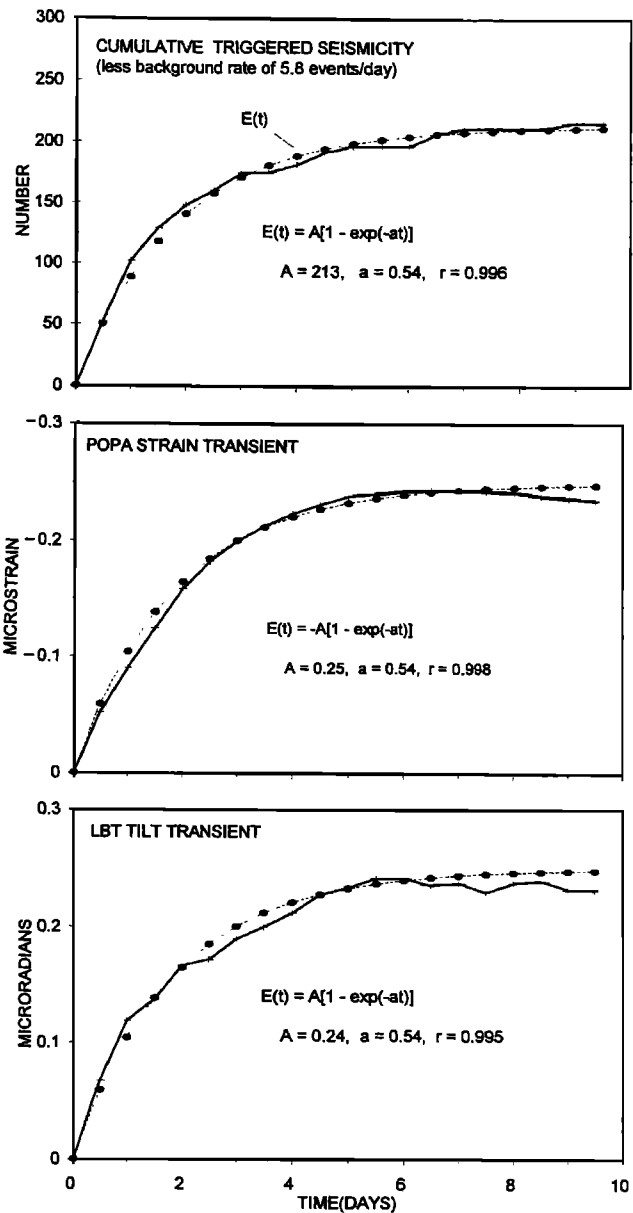


Figure 11. Comparison of the time evolution of the growth phase of the strain transient and cumulative number of triggered earthquakes for the first 10 days after Landers. (top) Cumulative number of triggered earthquakes (less a constant background rate of 5.8 events/d; see Figure 4). (middle) POPA dilatational strain transient (tides and annual trend removed, negative strain positive upward; see Figure 10). (bottom) E-W component of LBT tilt with tides removed. The exponential fit has the same time constant, $1/a = 1.8$ days, for all three curves. The quality of fit to each curve indicated by Parson's correlation coefficient r .

of renewed inflation of the resurgent dome that began in October 1989. As with the triggered response of the caldera to Landers, the cumulative deformation moment since 1989 exceeds the cumulative seismic moment of earthquakes within the caldera over the same time period by more than an order of magnitude.

On a regional scale, we note that strain transients with much the same form as those at POPA and LBT (but with no

reversal in sense and amplitudes of only 0.05–0.15 ppm) were recorded at the Pinon Flat Observatory (PFO [Wyatt *et al.*, 1994]), although these PFO strain transients were not accompanied by triggered seismicity. The Pinon Flat Observatory is just 70 km south of the Landers epicenter and thus within a source dimension of the mainshock. Similar strain transients were not detected by borehole dilatometers along the San Andreas fault at either Devil's Punchbowl, 130 km west of the mainshock epicenter, or at Parkfield, 400 km northwest of the epicenter [Johnston *et al.*, 1994].

Models for the Triggering Process

Summarizing from above, critical aspects of the caldera's response to the Landers earthquake that a viable model for the triggering process must satisfy include the following:

1. The triggered seismicity differed from ongoing activity only in that the entire seismogenic volume of the caldera was activated at once (Figure 5). Whatever the triggering process, it did not noticeably perturb local conditions in the brittle crust that have governed the spatial distribution, focal mechanisms, or frequency-magnitude distribution of earthquakes in the caldera over the last decade.
2. The cumulative moment of the triggered earthquakes was the equivalent of a single $M = 3.8$ earthquake ($M_0 = 2.4 \times 10^{22}$ dyn cm), and the dominant moment release occurred with $M = 3.2$ and 3.7 events at 17.6 and 20.0 hours after Landers, respectively. (The cumulative moment for intracaldera triggered seismicity is $M_0 = 0.9 \times 10^{22}$, or the equivalent of a $M = 3.5$ event.) The seismic slip represented by the cumulative moment of the triggered seismicity is too small by 2 orders of magnitude to produce the transient strain pulse recorded at POPA and LBT.
3. The cumulative number of triggered earthquakes grew with time as $N(t) = N_0(1 - e^{-at})$ against a background rate of 5.8 events/d with $N_0 = 213$ and $1/a = 1.8$ days. It appears as though the surge in triggered seismicity represents activity superimposed on a steady background seismicity rate of 5.8 events/d that had persisted for some 15 days prior to Landers and continued for several months afterwards (Figure 4).
4. The transient strain pulse detected by the POPA borehole dilatometer at the southwestern margin of the caldera and the LBT tiltmeter in the south central section of the caldera began abruptly as the dynamic waves from Landers passed through the caldera and grew in parallel with the cumulative number of triggered earthquakes as $f(t) = C(1 - e^{-at})$, with again $1/a = 1.8$ days. The compressional strain transient at POPA (a volume decrease of the rock matrix) peaked with an amplitude of 0.25 ppm after 6 days and gradually decayed over the next 20 days; the tilt transient at LBT peaked with a down-to-the-southeast tilt of 0.24 ppm also after 6 days and decayed over the next 5–10 days.
5. Measurements of baselines spanning the central section of the caldera showed no coherent horizontal strain exceeding the 0.4 ppm resolution of the two-color geodimeter [Johnston *et al.*, 1995] (Figure 3).
6. The confined aquifers in shallow (<1000 m) wells showed a transient response of variable amplitude to the dynamic strains of the crustal surface waves from Landers. Aside from a 12-cm drop in one well in the west moat (RDO-8) that persisted for at least 2 days, however, water levels in the wells showed no long-term offsets in excess of 1–2 cm [Roeloffs *et al.*, 1995].

Although these observations offer a host of tantalizing clues to the triggering process, the sparse spatial sampling of the transient strain pulse leaves the size and location of the sources producing the deformation underdetermined. The observations do, however, provide leverage for narrowing the range of viable models. We have dismissed the static stress change as an important factor because both observed and theoretical values are smaller by a factor of 10 than tidal stresses in the vicinity of the caldera. The observations also preclude two models involving the interaction of dynamic stresses with the local crust as playing a dominant role in the triggering process.

Two Precluded Models

Direct triggering of brittle slip by dynamic stresses. While direct triggering of brittle slip on local, critically stressed faults by favorably polarized dynamic stresses from the Landers mainshock may explain those earthquakes that occurred within the first few tens of seconds following the *S* wave arrival [Ruff, 1993; Anderson *et al.*, 1994], three observations indicate that direct triggering was not the dominant process in the triggered response of Long Valley caldera to the Landers mainshock. First, the cumulative seismic moment (and thus the cumulative seismic slip) of the triggered seismicity is much too small to produce the strain transients observed on the POPA dilatometer and the long-base tiltmeter (LBT). Second, the dominant moment release of the triggered seismicity occurred between 17 and 20 hours after Landers, and the peak in the strain transient occurred 4–6 days later, all long after the dynamic stresses had propagated through the area. Finally, the triggered surge appears to represent activity superimposed on a stable background seismicity rate and not simply an advance in the timing of earthquakes driven by a steady, long-term loading rate. (In the latter case, the triggered events would have used up the store of events that were about to occur, and an interval of reduced activity would follow until stresses returned to a critical level.)

Diffusive pore pressure increase. Direct triggering may occur if dynamic stresses produce leaks in compartments containing aqueous fluids under elevated pressure allowing these previously isolated fluids access to adjacent rock volumes. The resulting diffusion of elevated pore pressures into adjacent volumes will both reduce the effective strength of critically loaded faults (thereby triggering seismicity) and produce a poroelastic strain transient. For this process to produce the prompt onset of the strain transient recorded at POPA and LBT (Figure 8), however, requires high pore pressure compartments within a few hundred meters of the POPA and LBT instrument sites. In particular, if the emergent onset to a diffusion front is not to impart a noticeable delay in the convex upward growth of the poroelastic strain transient with respect to the arrival of peak dynamic stresses from the Landers mainshock, its duration (given by the characteristic diffusion time t_c) must be no more than a few hours ($t_c \leq 2 \times 10^4$ s). The corresponding diffusion length is $l_c \approx (t_c c)^{1/2}$, where c is the hydraulic diffusivity [Brace, 1980]. Taking a value of hydraulic diffusivity near the upper range of geophysically reasonable values for the crystalline crust ($c = 5 \text{ m}^2/\text{s}$, say [see Talwani *et al.*, 1984/85]) gives an upper bound on the diffusion length (the source-detector distance) of $l_c \leq 300$ m. This constraint thus precludes models requiring pore pressure diffusion from isolated, high-

fluid-pressure compartments located within the seismogenic volume of the crust (depths 4–8 km) as an explanation of the strain transient recorded at POPA and LBT. Furthermore, water well data in the caldera and vicinity offer little support for the existence of high-pressure compartments in the upper 1–2 km of crust that might be sufficiently close to either POPA or LBT to explain the strain transients (M. Sorey, personal communication, 1995).

We can also preclude poroelastic volume changes in the upper few hundred meters beneath the POPA and LBT driven by the hydraulic pumping action of passing surface waves [McHugh and Johnston, 1977] as an explanation for the strain transient observed at POPA and LBT. Under this model the poroelastic strain changes induced by the surface waves begin to relax immediately after the surface waves have passed as the temporarily elevated pore pressures decay by diffusion.

Four Conditionally Viable Models

Several models remain that, with qualified success, satisfy the constraints imposed by the seismic and deformation observations. These models include (1) a transient pressure increase in crustal magma bodies by advective overpressure [Linde *et al.*, 1994], (2) a transient pressure increase in fractures due to an upward surge in hydraulic fluids released by rupture of overpressured hydrothermal compartments during the passage of the large-amplitude surface waves [Johnston *et al.*, 1995], (3) liquifaction (relaxation) of a partially crystallized magma body [Hill *et al.*, 1993], (4) dike intrusion, and (5) aseismic slip (or creep) on local faults [Anderson *et al.*, 1994; Bodin and Gombert, 1994]. Fluids play a role in each of these models, and in this area of recent volcanism and geothermal activity the active fluids may be either aqueous or magmatic. Here we expand on the relaxing magma body and dike intrusion models and comment incidentally on the advective overpressure, hydraulic surge, and fault creep models, which are developed more completely elsewhere. Because the strain transients represent the dominant component of the triggered response, we pay particular attention to how well the deformation fields implied by these models satisfy the constraints imposed by the amplitude, sense, and temporal evolution of the deformation data. Our computations of the deformation fields for these models are based on Okada's [1985, 1992] code for point source dislocations in a half-space as modified for a moment tensor representation of the dislocation sources (B. Julian, personal communication, 1994).

Pressure increase in a magma body. Seismic activity and ground deformation in Long Valley caldera over the past decade are consistent with pressure increases in two small magma bodies in the upper crust beneath the caldera: one at a depth of 7–8 km beneath the central part of the resurgent dome [Langbein *et al.*, 1993] and the other at a shallow but poorly constrained depth beneath Mammoth Mountain at the southwestern margin of the caldera (see Figures 2 and 4) [Hill *et al.*, 1991; Sorey *et al.*, 1993; Pitt and Hill, 1994]. In addition, deformation patterns resolved by the two-color geodimeter data since 1989 admit the possibility of a weak pressure source at a depth of 10 km beneath the south moat roughly midway between POPA and LBT [Langbein *et al.*, 1995].

Linde *et al.* [1994] suggest that the dynamic waves from Landers triggered a transient pressure increase in one or

more of these magma bodies by advective overpressure. Under the idealized advective overpressure model described by Sahagian and Proussevitch [1992], pressure in an incompressible fluid of density ρ confined in a rigid container increases an amount $\Delta p = \rho gh$ as an included bubble rises a distance h , where g is the acceleration of gravity. In a compliant Earth, the pressure increase will be buffered by an associated volume increase ΔV , and Linde *et al.* [1994] estimate that the advective pressure increase in crustal magma bodies should be roughly a third of that predicted by the ideal (incompressible) case.

The temporal evolution of the strain transient under the Linde *et al.* [1994] model is governed by the competing effects of (1) the dynamics of bubbles of various sizes rising through a viscous (and probably stratified) magma and (2) the diffusion of the volatiles reaching the top of the magma body into the country rock and/or resorption of the volatile phase into the melt. Linde *et al.* [1994] suggest that the dynamic waves from Landers initiated the advective process by dislodging preexisting bubbles held down by surface tension forces. H. Kanamori (personal communication, 1994) pointed out to us another process that might serve to mobilize preexisting bubbles involves the rectified diffusion of mass (gas) into bubbles subjected to acoustic oscillations [Hsieh and Plesset, 1961; Crum and Hansen, 1982]. This process works in a volatile-saturated fluid because the surface area of a bubble is larger during the dilatational phase of a pressure wave (when the volatile phase exolves from the liquid phase) than during the compressional phase (when the volatile phase dissolves in the liquid phase) such that, on average, there is a net flux of mass (gas) into the bubble over several cycles.

Here we look more closely at the surface deformation expected from the volume increases associated with advective overpressurization. Figures 12a and 12b show surface deformation profiles due to an incremental volume increase ΔV in a spherically symmetric source (a Mogi source after Mogi [1957]) at depths of 7 and 3 km, respectively. Note that the deformation field for a Mogi source is symmetric about a vertical axis through the source. The dilatational strain becomes compressive ($\Delta < 0$) at distances beyond 1.4 source depths, although maximum amplitudes at these distances are 2 orders of magnitude smaller than the dilatational strains ($\Delta > 0$) at distances less than a source depth. Thus, to explain the sense of the strain transient observed at POPA and LBT, a Mogi source must be west of LBT and beyond 1.4 source depths from POPA. We find that a solitary source cannot produce both the sense and amplitude of the tilt transient observed at POPA and LBT without violating the 0.4-ppm upper bound on horizontal strains imposed by the two-color data. Simultaneous volume increases in the magma bodies beneath both the resurgent dome and Mammoth Mountain, however, will satisfy the deformation data. (Note that because the strain calculated for a finite baseline will in general differ from the continuous horizontal strain computed for an arbitrary point along the line, we plot horizontal surface displacements (in millimeters) rather than continuous strain in Figures 12 and 13. The strain appropriate for a baseline of the two-color geodimeter network coincident with the profile is thus the difference between the displacements at the endpoints of the line divided by the line length (in millimeters).

A volume increase of $\Delta V \approx 3 \times 10^{14} \text{ cm}^3$ (0.3 km³) in the

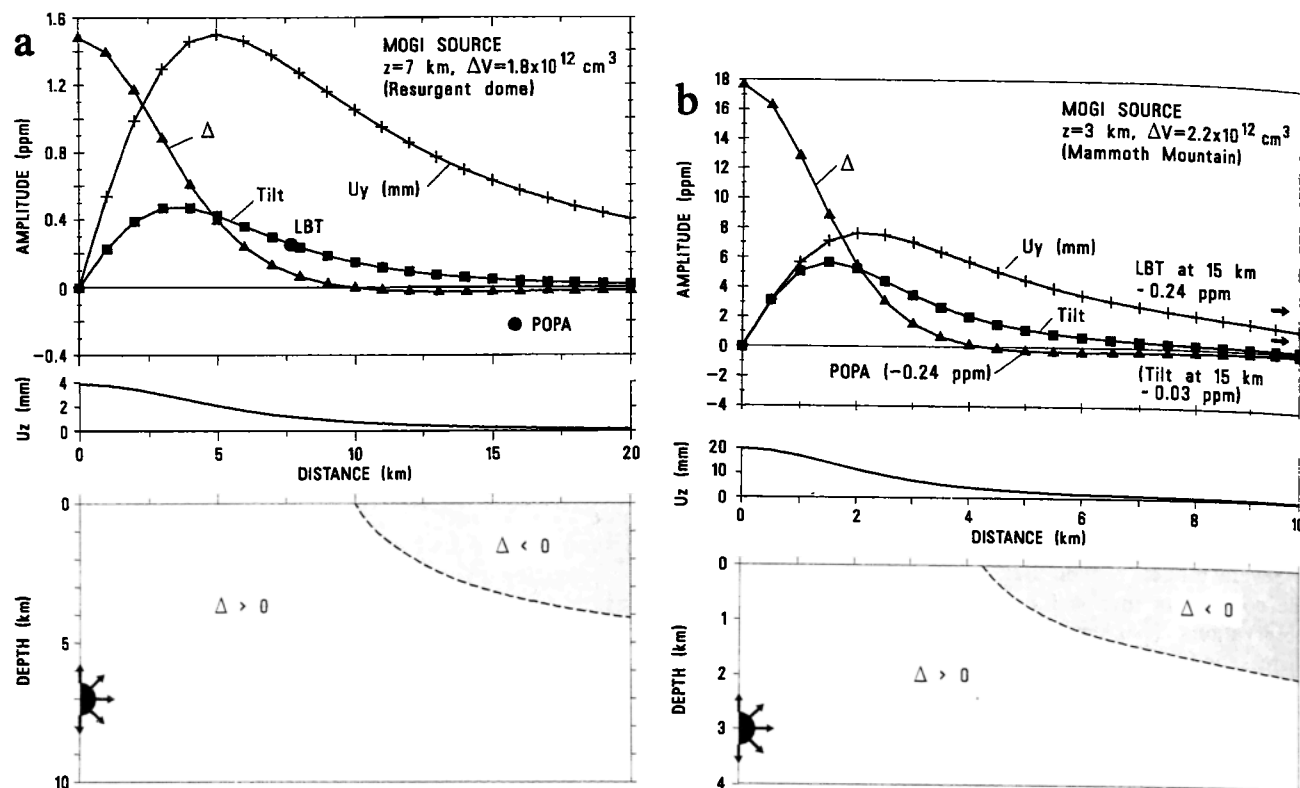


Figure 12. Deformation profiles for a compact inflation source (Mogi source). ΔV is volume increase required to fit observed tilt at LBT for source beneath resurgent dome (Figure 12a), and observed dilatational strain at POPA for source beneath Mammoth Mountain (Figure 12b). See Figure 5 for locations. (a) Source depth at 7 km beneath the resurgent dome coincident with inflation center driving long-term uplift of caldera (see Figure 2). (top) Surface strains (parts per million) along radial profile from source epicenter. Δ is dilatational strain, U_y is horizontal displacement (millimeters), and tilt is radial tilt. Solid circles show observed peak amplitudes of tilt and dilatational strain transient at LBT and POPA, respectively. (middle) Vertical displacement U_z (millimeters) (uplift positive). (bottom) Depth section through inflation source showing fields of positive and negative dilatational strain Δ . (b) Source depth at 3 km beneath Mammoth Mountain. Symbols same as in Figure 12a. Observed tilt at LBT, 15 km east of Mammoth Mountain, is 0.24 ppm; tilt from this source at 15 km is 0.03 ppm.

7-km-deep magma body beneath the resurgent dome accounts for most of the 60-cm uplift that has accumulated in the west central part of the caldera since 1980 [Langbein *et al.*, 1993]. An additional volume increase of $\Delta V = 1.8 \times 10^{12} \text{ cm}^3$ in this source can match the 0.24-ppm peak amplitude of the tilt transient at LBT at a distance of 7.5 km (Figure 12a), although the predicted tilt direction at LBT from this source is S55°E rather than the nearly due east tilt observed at LBT (see Figures 4 and 7). The associated horizontal displacements approach 1.6 mm, which corresponds to strains below the 0.4 ppm upper bound of the two-color geodimeter data. This resurgent dome source, however, produces a compressional strain an order of magnitude smaller than the observed $\Delta = -0.25$ ppm peak strain at POPA located 16 km to the west-southwest.

POPA is just 5 km west of the summit of Mammoth Mountain, and a volume source associated with a magma body beneath Mammoth Mountain must be no deeper than about 3 km for POPA to be within the compressional strain field (Figure 12b). To produce the $\Delta = -0.24$ ppm peak amplitude of the strain transient observed at POPA requires a volume change $\Delta V = 2.2 \times 10^{12} \text{ cm}^3$ at a depth of 3 km. The tilt from this source at a distance of 15 km to the east,

however, is only ≈ 0.03 ppm, or an order of magnitude below the peak tilt amplitude observed at LBT. The lack of additional deformation instrumentation in the vicinity of Mammoth Mountain leaves unanswered whether the large strains predicted for the epicentral region of this shallow source were realized following the Landers earthquake. In any case, the strain transient at POPA was not accompanied by a surge in seismicity beneath Mammoth Mountain.

Note that at distances beyond 8 km from the 3-km-deep source (Figure 12b), the dilatational strain is negative and the tilt and dilatational strain curves have comparable amplitudes. Thus a shallow volume source beneath the south moat midway between POPA and LBT with $\Delta V \approx 3 \times 10^{12} \text{ cm}^3$ would match the sense and amplitude of the strain transients detected at these sites. The large horizontal displacements produced by this shallow source approach 10 mm and would be clearly evident in the two-color geodimeter data following the Landers earthquake.

We note two intensive properties associated with a volume change in a Mogi source. The effective moment of the source is $M_0 = k\Delta V$, where k is the bulk modulus of the surrounding medium [Aki and Richards, 1980, p. 60]. For $k = 5 \times 10^{11} \text{ dyn cm}^{-2}$, the effective moments for the

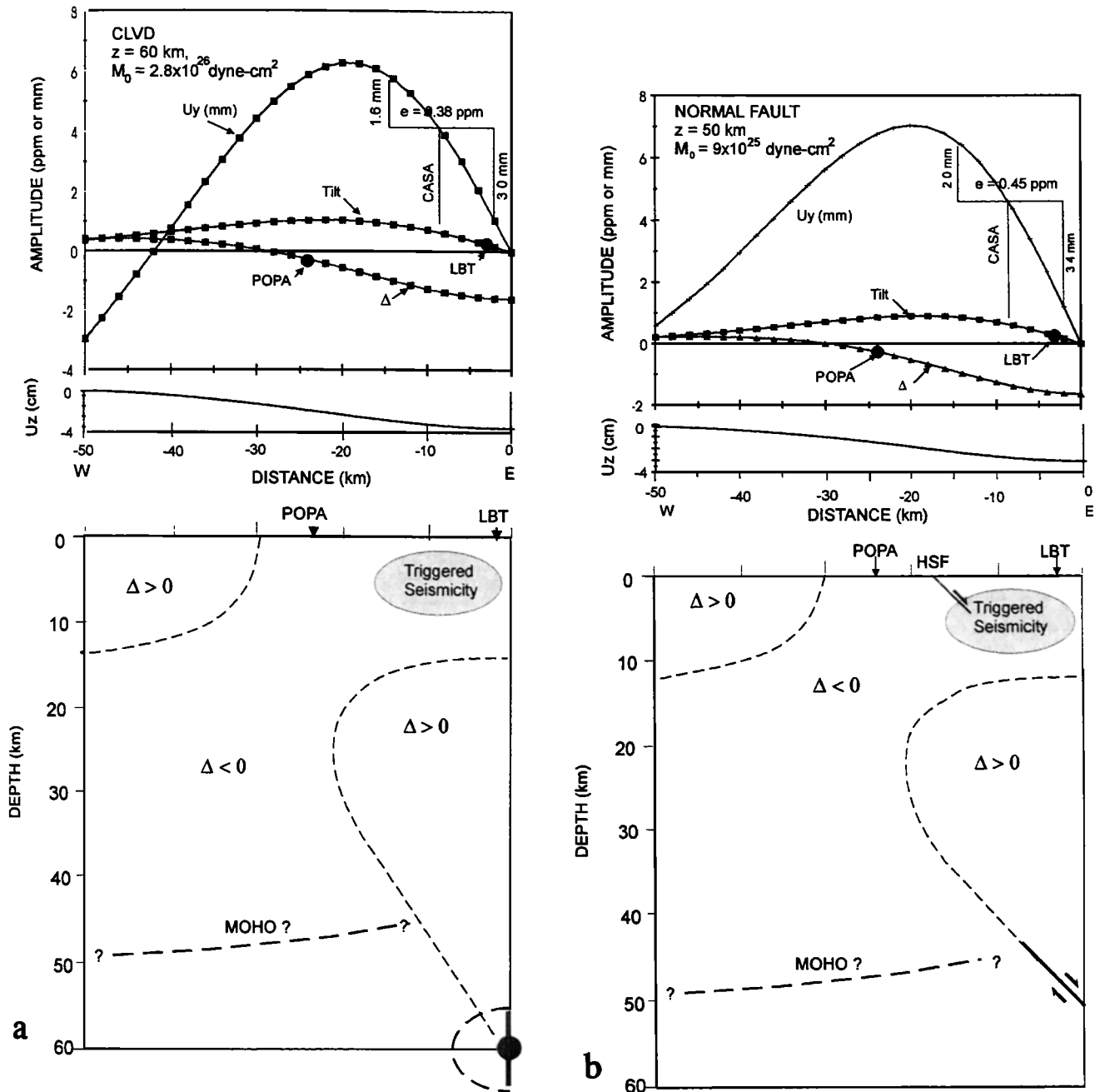


Figure 13. Deformation profiles for (a) a relaxing magma body or dike intrusion (represented by a CLVD point source) centered at 60 km and (b) slip on a normal fault centered at 50 km. Profiles extend west from source epicenters in the direction of maximum regional extension (the plane of the least principal horizontal stress). Conventions same as in Figure 12. (top) Surface strains (parts per million) and horizontal displacement U_y (millimeters). Vertical line CASA shows position of two-color geodimeter instrument site and horizontal line indicates span of the two-color network along the profile. Short vertical lines show predicted length changes of baselines with respect to CASA, which correspond to average contractional strains of 0.38 to 0.45 ppm across the two-color network. (middle) Vertical displacement U_z (centimeters) (uplift positive). (bottom) Depth section showing fields of positive and negative dilatational strain Δ . Stippled area indicates approximate volume of triggered seismicity. Dashed ellipse and shaded volume in Figure 13a represent relaxing magma body and dike intrusion, respectively. Heavy line in Figure 13b represents normal fault. HSF in Figure 13b is approximate position westernmost range front normal fault (Hartly Springs fault) in the vicinity of the caldera [Bailey, 1989].

resurgent dome and Mammoth Mountain sources in Figure 12 are $M_0 \approx 8 \times 10^{23}$ dyn cm and $M_0 = 1 \times 10^{24}$ dyn cm, respectively. Recall that the cumulative moment of the triggered seismicity is just $\sum M_0 = 2.4 \times 10^{22}$ dyn cm (see Figure 4), which is more than an order of magnitude smaller than either of these volume sources. The corresponding internal pressure increase is

$$\Delta P = \frac{4\mu U_z(0)z^2}{3a^3} \quad (4)$$

where μ is the shear modulus, $U_z(0)$ is the vertical displacement directly over the source, z is the source depth, and a is the source radius [Mogi, 1958]. Taking $\mu = 3 \times 10^{11}$ dyn cm⁻² and $U_z(0) = 0.4$ cm from Figure 12a, a pressure increase of $\Delta P \approx 150$ bars within a magma body with a radius of 0.8 km will produce the deformation field in Figure 12a. This is roughly a factor of 4 smaller than ΔP predicted by the idealized advective overpressure model and in general agreement with the estimate of Linde *et al.* [1994]. Because of its shallower depth, ΔP for the Mammoth Mountain source will be slightly smaller (by a factor of 0.92) for a given source volume than for the resurgent dome source (see equation (4)).

Tomographic studies of the velocity and attenuation structure beneath the caldera indicate that the dimensions of magma bodies in the upper 8–10 km of the crust are at most a few kilometers [Kissling, 1988; Dawson *et al.*, 1990; Romero *et al.*, 1993; Sanders, 1993; Steck and Prothero, 1994; Ponko and Sanders, 1994]. A minimum size for the volume V_{\min} of the resurgent dome magma body is that required to account for the 60-cm uplift of the resurgent dome since 1979, or $V_{\min} \approx 3 \times 10^{14}$ cm³ (0.3 km³ and a diameter of 0.4 km). The corresponding upper bound on the fractional volume increase for the resurgent dome source in Figure 12a is $\Delta V/V_{\min} \approx 0.006$. Gerlach *et al.* [1994] estimate that crustal magmas contain 6–8 vol % of volatiles. Accordingly, if the strain transient is indeed driven by mobilized volatiles (advective overpressure) in crustal magma bodies, it seems that the dynamic strains from Landers mobilized only a fraction of the potentially available volatile content in the magma.

A nagging issue with this model is that we require volume increases in two, spatially distinct magma bodies to satisfy the deformation data and, further, that the two magma bodies respond with a common time constant to the dynamic strains from the Landers earthquakes (at least through the first six days). An implication is that the two bodies have a similar size, composition, and state. Recent activity beneath the caldera and Mammoth Mountain admit this possibility but we lack data with the resolution to corroborate the details.

Hydraulic pressure surge. Johnston *et al.* [1995] propose a hydraulic surge model that involves volume increases in the shallow crust driven by increased pore pressures and its subsequent decay by diffusion. They propose that the large dynamic strains propagating with the Landers surface waves ruptured compartments of super hydrostatic fluid pressures, which are commonly encountered in volcanic and geothermal regions [Fournier, 1991]. They suggest that the result was an upward surge of fluids in the crust beneath the caldera by hydraulic fracturing, similar to the process postulated by Byerlee [1993] for the cascading rupture of high-

pore-pressure fluid compartments in a fault zone. We used a dislocation representation of an opening crack to model the shallow component of this process and a compensated linear vector dipole (CLVD) to model a combined volume collapse and opening crack system [see Julian, 1983] to explore the deformation associated with this process. As with the advective overpressure model, we find that a single source (using either representation) within the upper 20–30 km of the crust cannot explain all of the deformation data. Because the hydraulic surge model requires a wide distribution of sources through the volume of triggered seismicity, however, a distribution of shallow sources can be found that will satisfy the available deformation data. Thus this model may also appeal to the coincidence that the sources local to POPA and LBT happen to evolve with the same time history.

Relaxation of a partially crystallized magma body or dike intrusion. A magma body with a relatively small melt fraction transmits shear waves from local earthquakes and thus behaves as a solid under small, high-frequency strains. The large, low-frequency strains associated with the shear wave pulse and crustal surface waves from the Landers mainshock may have partially liquified such a body, thereby releasing some of the differential stress supported by the solid phase. Alternatively, the large dynamic stresses from Landers may have induced a magmatic intrusion by disrupting the cohesive strength of an incipient or partially healed dike adjacent to a crustal or upper mantle magma source. Candidates for such a body in the Long Valley region include, in addition to the shallow magma bodies beneath the resurgent dome and Mammoth Mountain described above, the volume of low P wave velocity material that underlies the west central part of the caldera at depths between 10 and 20 km [Dawson *et al.*, 1990; Steck and Prothero, 1994] and a volume spanning a similar depth range centered just southwest of Mammoth Mountain that has produced recurring long-period (LP) volcanic earthquakes since 1989 [Pitt and Hill, 1994]. In addition, we consider a magma body near the base of the crust beneath the caldera that may be the lower crustal root the Long Valley magmatic system [Bailey, 1982] and that coincides with a deep, low P wave velocity region described by Dawson *et al.* [1990].

To first order, the deformation produced by either a relaxing magma body (loss of rigidity in a solid inclusion) or dike intrusion can be modeled using a compensated linear vector dipole (CLVD) source [Knopoff and Randall, 1970; Julian, 1983]. Neither of these processes involves a net volume change within the source volume. A spherical inclusion (magma body) relaxing in a regional tectonic stress regime will deform into an ellipsoid with major and minor axes in the direction of the least and greatest principal stresses, respectively. In the case of dike intrusion, mass transport is accommodated by a local volume increase as a dike opens in the direction of the least principal stress and a compensating volume decrease (here assumed to be isotropic) of a nearby region from which the fluid phase was evacuated. The tectonic stress regime of the eastern Sierra Nevada–western Great Basin is characterized by a mix of normal and strike-slip faulting and a horizontal least principal stress [see Zoback and Zoback, 1991]. The least principal stress direction in the vicinity of Long Valley caldera varies from east-west to northeast-southwest (see Figure 6) [Hill *et al.*, 1991; Langbein *et al.*, 1993; Moos and Zoback, 1993].

Figure 13a illustrates the deformation of an elastic half-space due to either a relaxing magma body or dike intrusion centered at a depth of 60 km represented by a CLVD source relaxing in an east-west extensional stress field. The deformation is shown for a vertical plane through the source in the direction of regional extension (the least principal stress direction). The free surface over this source is warped downward to a distance of about 0.8 source depths from the epicenter so that the tilt within this range is toward the epicenter. At 1.3 source depths (not shown), flexure of the free surface reverses sense. Beyond 1.3 source depths, the tilts are small and away from the epicenter. The downward-warped surface over the epicenter places the near-surface rocks in compression with the result that the dilatational strain at the surface is negative ($\Delta < 0$) to distances of 0.5 source depths from the epicenter. Beyond 3 source depths, the dilatational strain becomes negative again, but at these distances the strain amplitudes are 2–3 orders of magnitude below those in the vicinity of the source.

Again we find that a single deformation source in the crustal volume that includes the recognized magma bodies or zones of low P wave velocity beneath the western and central sections of the caldera (depths ≤ 25 km) cannot simultaneously match the sense and amplitudes of the strain transient recorded at POPA and LBT and the 0.2- to 0.4-ppm upper bound on horizontal strain from the two-color geodimeter data. A CLVD source centered at a depth of 10 km beneath the southwest flank of Mammoth Mountain (coincident with the crustal volume producing long-period volcanic earthquakes [Pitt and Hill, 1994]), for example, can readily account for the -0.25 ppm dilatational strain at POPA, but the tilt amplitude at LBT from this source is only 0.006 ppm. A CLVD source coincident with either the 3-km-deep source beneath Mammoth Mountain or the 7-km-deep source beneath the resurgent dome will produce positive dilatational strain at POPA. A body centered at a depth of 20 km beneath the western margin of the resurgent dome coincident with the low P wave velocity volume described by Dawson *et al.* [1990] would produce the correct strain sense at POPA but not at LBT.

One site (there may be others) for a CLVD source capable of producing strains that match both the sense and amplitude of the transients at POPA and LBT without violating the ≈ 0.4 -ppm constraint on horizontal strain imposed by the two-color geodimeter data is centered 2–3 km east of LBT at a depth of 60 km (Figure 13a). To produce the observed 0.24-ppm strain amplitudes at this site requires a source moment of $M_0 = 2.8 \times 10^{26}$ dyn cm². This corresponds to deformation of an initially spherical body with a radius of 8 km into an ellipsoid with the vertical dimension shortened by 60 cm and the horizontal dimension lengthened by 60 cm (in the direction regional extension) or a 2-m-wide dike some 20 km long and 20 km high (using $M_0 = 4/3\mu\Delta V$ for a CLVD and taking $\mu = 3 \times 10^{11}$ dyn cm⁻²). A magma body or intrusion at this location would be just below the base of the crust [see Fuis and Mooney, 1990], and it would coincide with the roots of the Long Valley magmatic system suggested by Bailey [1982]. At this depth, the shear wave pulse will likely carry the triggering strains rather than the crustal surface waves [see Gomberg and Bodin, 1994; Spudich *et al.*, 1995]. Results of the teleseismic tomography studies by Dawson *et al.* [1990] and Steck and Prothero [1994] both show a zone of relatively low P wave velocities in this depth

range beneath the eastern margin of the resurgent dome. In map view, the Dawson *et al.* [1990] results indicate that this low-velocity zone is elongated in a northward direction consistent with a magma body or dike with its long axis in a north-south direction. (Note that we do not attempt to account for finite source dimensions in our calculation of the deformation field. The moment for this 60-km-deep CLVD source is sufficiently large, however, that source dimensions may approach a third to half a source depth and thus begin to influence details of the deformation field and the specific source location.)

The temporal form of the growth of the strain transient produced by the CLVD model will be governed by the relaxation time of the partially liquified magma body or the intrusion time history of the dike. Equation (3) which describes the relaxation of a Kelvin body (a spring and dashpot in parallel) as well as the growth phase of the strain transient and the cumulative number of triggered earthquakes with time (Figure 11), provides a reasonable approximation to the time function for the relaxation of a viscous magma body in an elastic crust (i.e., the time required for magma to approach hydrostatic equilibrium). In this case the time constant, $1/a = \nu/k$, where ν is the effective viscosity of the magma and k is the elastic stiffness of the surrounding crust. The relaxation time of ≈ 2 days for the growth phase of both the strain transient and the cumulative seismicity (Figure 11) together with an elastic stiffness for crustal rocks $\approx 10^{11}$ dyn cm⁻², implies a viscosity of the partially liquified magma body $\approx 10^{16}$ P. This value is 3 orders of magnitude below that for the relatively soft asthenosphere beneath the Great Basin ($\approx 10^{19}$ P), and it may well represent the effective viscosity of a crystalline mush with a higher percentage of basaltic melt than the surrounding sections of the Basin and Range upper mantle.

To a first approximation, the time constant for the local volume increase associated with dike growth depends on fluid viscosity, the square of the dike aspect ratio, and the pressure difference driving the intrusion [Julian and Sipkin, 1985]. Assuming a dike aspect ratio in the range 10^{-4} to 10^{-2} and a driving pressure of a few hundred bars, for example, the ≈ 2 -day time constant for the growth phase of the strain transient suggests melt viscosities in the range 10^4 to 10^8 P. This compares with viscosities of 10^2 to 10^4 P for crystal-free basaltic melts [Murase and McBirney, 1973]. The deformation field for the well-documented dike intrusion associated with the 1989 Off-Ito eruption in Japan [Okada and Yamamoto, 1991] developed with an exponential-like time history remarkably similar in form and duration to the triggered strain transient in Long Valley caldera illustrated in Figure 8. This dike intrusion model admits the interesting possibility that large, regional earthquakes can trigger an episodic recharge of deep roots to crustal magmatic systems.

A potential weakness with deep, relaxing-magma-body and dike-intrusion models lies in the relation between the strain changes produced by the deep deformation source and the triggered seismicity in the overlying crust. As illustrated in Figure 13, the triggered seismicity falls within the volume of negative dilatational strain ($\Delta < 0$) beneath the downward-warped free surface. Within this volume, the horizontal stress components increase while the vertical component decreases. These stress changes move the Coulomb failure function [Stein *et al.*, 1992] toward failure by 0.1 to 0.2 bar on west dipping normal faults and away from failure by a

comparable amount on east dipping normal and vertical strike-slip faults (calculations based on a coefficient of friction, $\mu = 0.75$, and a saturated, undrained medium (R. Simpson, personal communication, 1994). Mapped faults spanning the resurgent dome show a mix of both west and east dipping normal faults [Bailey, 1989], and most of the triggered earthquakes show a significant component of normal slip (Figure 6). Furthermore, we know that, on average, the ambient stress field must be near the failure threshold on local faults because of the persistent seismicity prior to and following Landers (Figure 4). Thus it appears that, at least in principle, the small stress changes associated with this deep deformation source are capable of pushing the seismogenic volume in the direction of an increased failure (seismicity) rate.

Aseismic slip on midcrustal faults. Anderson *et al.* [1994] and Bodin and Gombert [1994] suggest that deformation associated with aseismic slip (creep) on local faults at midcrustal depths initiated by the large, low-frequency shear pulse from Landers may have induced much of the remotely triggered seismicity. We find that the deformation fields from slip at shallow to midcrustal depths (≤ 25 km) on the major, recently active faults beneath and adjacent to the caldera fail to match the strain data. The deformation field due to slip on a normal fault with a 45° dip is grossly similar to that produced by a CLVD (compare Figures 13a and 13b). Such a source anywhere beneath the western half of the caldera, however, fails to match the sense and amplitude of the observed strain at either or both POPA or LBT. As illustrated in Figure 13b, however, the deformation field for creep on a normal fault at a depth of 45–50 km beneath the east central part of the caldera will match the strain observations. At this depth, of course, a “fault” is well below the base of the brittle crust. Conceivably, the Sierran range front fault system penetrates the aseismic, lower crust as a zone of distributed, plastic shear. The surface traces of the major range front faults in the vicinity of the caldera are less than 20 km west of this deep source, however, and their fault planes would have to maintain average dips in excess of 80° to intersect the source at a depth of 50 km (see Figure 13b). Such a configuration is contrary to the geometry of most normal faults. The deformation field due to a northeast striking dextral strike-slip fault (or a northwest striking sinistral fault) in the lower crust (depth 45–50 km) located midway between POPA and LBT can also satisfy the strain data. Slip on such a fault implies an east-west orientation for greatest principal stress, however, which is opposite to that expected for a region dominated by east-west extension.

Poroelastic decay. By itself, the stress drop resulting from the liquifaction of a partially crystallized magma body, dike intrusion, or fault slip under the regional stress field will result in a unidirectional, permanent offset in the displacement and strain fields. To account for the observed decay of the strain transients requires a second process such as, say, the poroelastic response of a fluid-saturated crust to the deformation source.

Rice and Cleary [1976] describe the behavior of fluid-saturated poroelastic media for a variety of problems, and we base the following qualitative argument on their results. Consider the dilatational strain field produced by a CLVD source or slip on a normal fault imposed on a water-saturated, poroelastic crust (Figure 14). We assume that at the shallow depths ($z < 200$ m) in which POPA and LBT are

installed, the rocks behave as a drained medium. For a constant hydraulic diffusivity c , diffusion lengths and times will increase systematically with depth such that the poroelastic system behaves progressively more like an undrained medium with increasing depth (see Roeloffs *et al.*, 1989). Taking a hydraulic diffusivity near the upper range appropriate for crystalline crustal rocks ($c \approx 5 \text{ m}^2/\text{s}$ [Tawani *et al.*, 1984/85]); for example, the characteristic diffusion time at $z = 200$ m will be $t_c = 42$ minutes and at $z = 3$ km it will be $t_c = 4.5$ days (the diffusion time for relaxation of the strain transient for equation (2) as illustrated in Figure 10). Thus, at depths below ≈ 1 km where the diffusion times are comparable to or longer than the ≈ 2 -day relaxation time of the deformation source, the crust will behave as an undrained medium. At these depths, initial pore pressure changes will be opposite to the local dilatational strain changes in the undrained region (B and C in Figure 14). Pore fluids will diffuse down the induced pressure gradients (in the direction of the small arrows in Figure 14) resulting in further expansion of the rock matrix in the $\Delta > 0$ volume above the source (C in Figure 14). Gradual expansion of this volume will in turn partially relax the overlying downward warped surface and the negative dilatational strain in the drained surface layer (D in Figure 14). (At a minimum, the shallow crust in the vicinity of POPA must behave as a drained volume for this process to explain the observed reversal in the dilatational strain transient.) Under this process the dilatational strains retain a permanent offset proportional to the purely elastic response to the source after pore pressures in the poroelastic medium return to equilibrium. The transient decay would presumably have the form of equation (2) (Figure 10) with the error function representing a solution to the diffusion equation.

Discussion

Of the models considered above, either the relaxing magma body or dike intrusion at a depth of approximately 60 km beneath the east central part of the caldera has the distinct advantage of explaining the available deformation data with a single deformation source. The position of this source near the base of the crust is consistent with the deep root of the Long Valley caldera–Mono Craters magmatic system [Bailey, 1982] and a zone of relatively low P wave velocities [Dawson *et al.*, 1990; Steck and Prothro, 1994]. Furthermore, it seems likely that much of the actively extending margin of the Basin and Range province includes deep zones of basaltic magma (or partial melt) drawn into the lower crust or upper-most mantle as part of the mass balance accompanying crustal extension [Lachenbruch *et al.*, 1976; Wilshire and Kirby, 1989]. Thus the relaxing magma body or dike intrusion models need not be special to the triggered response of Long Valley caldera. Most of the seismicity triggered by the Landers earthquake was concentrated along the margins of the Basin and Range province [Hill *et al.*, 1993], and it is plausible that the triggered seismicity was driven by local strain transients accompanying the response of underlying, lower crustal magma bodies to the large shear pulse from the Landers mainshock. If this model is correct, it suggests that significant influx of basaltic magma into the deep roots of crustal magmatic system occurs episodically in response to large, regional earthquakes. This in turn offers a specific link between regional tectonism and magmatism. A

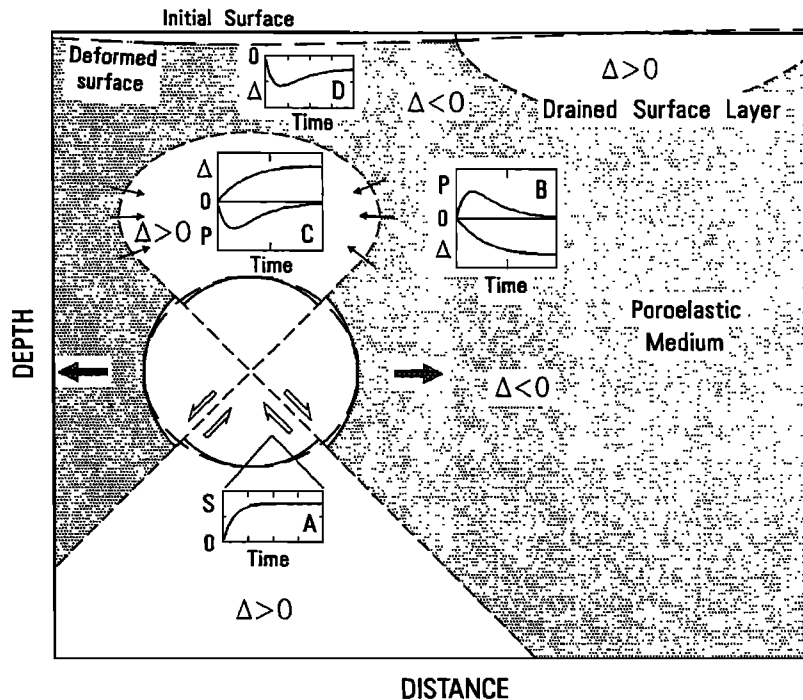


Figure 14. Diagram illustrating anticipated response of poroelastic crust to relaxing magma body, dike intrusion, or slip on normal fault. Depth section is parallel with direction of regional tectonic extension (shaded arrows). Dashed lines separate fields of positive (expansive) and negative (contractive) dilatational strain, Δ , resulting from source deformation. Insets show time history of A, source relaxation function; B, pore pressure $P(t)$ and dilatational strain $\Delta(t)$ in undrained volume where $\Delta < 0$; C, $P(t)$ and $\Delta(t)$ in undrained volume where $\Delta > 0$; and D, $\Delta(t)$ in drained surface layer where $\Delta < 0$. (Compare with strain fields for models in Figure 13.)

potential flaw in the relaxing magma body or dike intrusion models is that the small stress changes from the deep source nudge the local stress field only marginally (≤ 0.3 bar) toward Coulomb failure within the seismogenic volume. King *et al.* [1994], however, find that Coulomb stress changes of less than one-half bar appear sufficient to trigger aftershocks to moderate earthquakes.

The model proposed by Linde *et al.* [1994] involving a transient pressure increase in shallow magma bodies beneath Mammoth Mountain and the resurgent dome by advective overpressure remains an intriguing contender for the triggering process. Transient inflation of the resurgent dome magma body provides a natural explanation for the surge in triggered seismicity; it simply represents a brief acceleration of a process in the caldera that has been ongoing since 1980 [Langbein *et al.*, 1993]. The absence of triggered seismicity in the vicinity of the Mammoth Mountain magma body, however, remains a puzzle under this model. To explain the coincidence of a common deformation function for spatially distinct magma bodies under this model requires the (not entirely unreasonable) assumption that both magma bodies happen to have a common size and state.

An increase in pore pressure in the seismogenic crust according to the hydraulic surge model readily explains the triggered seismicity within the caldera, and the latitude afforded in the spatial distribution of transient volume increases in the shallow crust allows ample flexibility in meeting the constraints of the deformation data [Johnston *et*

al., 1995]. As with the advective overpressure model, however, the absence of triggered seismicity beneath Mammoth Mountain associated with a local source for the dilatational strain transient at POPA is puzzling.

Aseismic slip on any of the recognized major faults in the vicinity of the caldera does not seem promising as a coherent explanation for the triggered response in the caldera. Although aseismic slip on a normal fault centered at 50 km beneath the caldera can account for the sense and amplitude of the recorded strain transient, a fault at that location lacks a plausible geometric relation to the surface traces of the Sierra Nevada range front faults less than 15 km to the west. Aseismic slip on a strike-slip fault at a similar depth beneath the caldera can also account for the strain data but with kinematics that require east-west contraction rather than extension.

Each of these models involves the release of some form of stored energy that must be recharged before the system is susceptible to a recurrence of the triggering process. The advective overpressure model requires an infusion of volatile-rich magma or a buildup of volatiles in a magma chamber through continued crystal fractionation (or perhaps a buildup of the vapor phase in shallow hydrothermal systems). The relaxing magma body, dike intrusion, and fault slip models all require the accumulation of strain energy from long-term tectonic loading, and, of course, a recently relaxed magma body requires time to partially set before it can begin to support a differential stress. The hydraulic surge model requires that the ruptured fluid compartments reseal sufficiently to support a subsequent build up internal of fluid

pressures. The timescale for the recharging processes may range from weeks to centuries depending on the model, the local crustal environment, and regional deformation rates. At one extreme, both bubbles and permeability seals can re-form quickly (weeks) in crustal hydrothermal systems [Fournier, 1991; Moore et al., 1994]. This short recharge time for hydrothermal systems may account for the frequent occurrence of bursts in seismicity at The Geysers geothermal area in California triggered by strong, regional earthquakes as documented by M. A. Stark and S. D. Davis (Remotely triggered microearthquakes at The Geysers geothermal field, California, submitted to *Geophysical Research Letters*, 1994). At the other extreme, the recharge process for the relaxing magma body model probably requires decades to centuries.

Conclusions

Fluids play a distinct role in each of the four models described above for the triggered response of Long Valley caldera to the Landers mainshock, and each of these models carries different implication for the role of fluids in the mechanical behavior of the crust. We are attracted to the relaxing magma body and dike intrusion models because of their relative simplicity (a single deformation source explains the available deformation data), because volumes of partial melt probably reside near the base of the crust beneath most of the areas that responded with triggered seismicity, and because of the implication they carry for a temporal connection between large regional earthquakes and episodes of crustal magmatism. With the equivalent of only three data points defining the deformation field, however, we are faced with a severely underdetermined problem, and our ability to discriminate between any of these models is limited.

The widespread seismicity triggered by the Landers earthquake was a surprising, important, and probably rare event. Were it not for the geophysical monitoring program focused on volcanic unrest in Long Valley caldera, we would have completely missed the fact that at least at one site of remotely triggered seismicity, a strain transient was the dominant mode of the triggered response. In the absence of a more regional distribution of continuous strain monitoring instruments (bore hole strain meters, long-base tiltmeters, and pressure transducers in stable water wells of opportunity) with sufficient sensitivity to track solid Earth tides, we are likely to be in a similar situation when next the Earth offers an opportunity to test these models with a repeat experiment.

Acknowledgments. We are grateful to Joan Gomberg, Bill Ellsworth, Stuart Rojstaczer, an anonymous referee, and Steve Hickman as Associate Editor for their thorough and thoughtful reviews of earlier versions of this manuscript. We thank Bob Simpson for providing critical (and colorful) Coulomb failure calculations.

References

- Aki, K., and P. G. Richards, *Quantitative Seismology, Theory and Methods*, 932 pp., W. H. Freeman, New York, 1980.
- Anderson, J. G., J. N. Brune, J. Louie, Y. Zeng, M. Savage, G. Yu, Q. Chen, and D. dePolo, Seismicity in the western Great Basin apparently triggered by the Landers, California, earthquake, June 28, 1992, *Bull. Seismol. Soc. Am.*, **84**, 863–891, 1994.
- Bailey, R. A., Other potential eruption centers in California: Long Valley, Mono Lake, Coso, and Clear Lake volcanic fields, *Calif. Div. Mines Geol. Spec. Publ.*, **63**, 17–28, 1982.
- Bailey, R. A., Geologic map of Long Valley caldera, Mono-Inyo Craters volcanic chain and vicinity, eastern California, *U.S. Geol. Surv. Map, I-1933*, 2 sheets and 11 pp., 1989.
- Bailey, R. A., and D. P. Hill, Magmatic unrest at Long Valley caldera, California, 1980–1990, *Geosci. Can.*, **17**, 175–178, 1990.
- Bailey, R. A., G. B. Dalrymple, and M. A. Lanphere, Volcanism, structure, and geochronology of Long Valley caldera, Mono County, California, *J. Geophys. Res.*, **81**, 725–744, 1976.
- Behr, G., R. Bilham, and S. Whitehead, Biaxial Michelson tiltmeter at Mammoth Lakes (abstract), *Eos Trans. AGU*, **70**, 1058, 1989.
- Bodin, P., and J. Gomberg, Triggered seismicity and deformation between the Landers, California, and Little Skull Mountain, Nevada, earthquakes, *Bull. Seismol. Soc. Am.*, **84**, 835–843, 1994.
- Brace, W. F., Permeability of crystalline and argillaceous rocks, *Int. J. Rock Mech. Min. Soc. Geomech. Abstr.*, **17**, 241–251, 1980.
- Byerlee, J., Model for episodic flow of high pressure water in fault zones before earthquakes, *Geology*, **21**, 303–306, 1993.
- Crum, L. A., and G. M. Hansen, Generalized equations for rectified diffusion, *J. Acoust. Soc. Am.*, **72**, 1586–1592, 1982.
- Dawson, P. B., J. R. Evans, and H. M. Iyer, Teleseismic tomography of the compressional wave velocity structure beneath the Long Valley region, California, *J. Geophys. Res.*, **95**, 11,021–11,050, 1990.
- Farrar, C. D., M. L. Sorey, S. A. Rojstaczer, C. J. Janik, R. H. Marinert, and T. L. Winnett, Hydrologic and geochemical monitoring in Long Valley caldera, Mono County, California, *U.S. Geol. Surv. Water Resour. Invest. Rep.*, **85-4183**, 137 pp., 1985.
- Fournier, R. O., The transition from hydrothermal to greater than hydrostatic fluid pressure in presently active hydrothermal systems in crystalline rock, *Geophys. Res. Lett.*, **18**, 955–958, 1991.
- Fuis, G. S., and W. D. Mooney, Lithospheric structure and tectonics from seismic-refraction and other data, in *The San Andreas Fault System*, edited by R. E. Wallace, *U.S. Geol. Surv. Prof. Pap.*, **1515**, 207–236, 1990.
- Gerlach, T. M., H. R. Westrich, and R. B. Symonds, Pre-eruption vapor saturation in magma of the climactic Mount Pinatubo eruption: Source of the giant stratospheric sulfur dioxide cloud, in *The 1991–1992 Eruption of Mount Pinatubo, Philippines*, edited by R. S. Punongbayan and C. G. Newhall, *U.S. Geol. Surv. Prof. Pap.*, in press, 1995.
- Gomberg, J., and P. Bodin, Triggering of the $M_s = 5.4$ Little Skull Mountain, Nevada, earthquake with dynamic strains, *Bull. Seismol. Soc. Am.*, **84**, 844–853, 1994.
- Hill, D. P., Monitoring unrest in a large silicic caldera, the Long Valley-Inyo craters volcanic chain complex in east-central California, *Bull. Volcanol.*, **47**, 371–395, 1984.
- Hill, D. P., Temperatures at the base of the seismogenic crust beneath Long Valley caldera, California, and the Phlegrean Fields caldera, Italy, in *Volcanic Seismology*, edited by P. Gasparini, R. Scarpa, and K. Aki, pp. 432–461, Springer-Verlag, New York, 1993.
- Hill, D. P., R. A. Bailey, and A. S. Ryall, Active tectonic and magmatic processes beneath Long Valley caldera, eastern California: a summary, *J. Geophys. Res.*, **90**, 11,111–11,120, 1985.
- Hill, D. P., W. L. Ellsworth, M. J. S. Johnston, J. O. Langbein, D. H. Oppenheimer, A. M. Pitt, P. A. Reasenber, M. L. Sorey, and S. R. McNutt, The 1989 earthquake swarm beneath Mammoth Mountain, California: An initial look at the 4 May through 30 September activity, *Bull. Seismol. Soc. Am.*, **80**, 325–339, 1991.
- Hill, D. P., et al., Seismicity remotely triggered by the magnitude 7.3 Landers, California, earthquake, *Science*, **260**, 1617–1623, 1993.
- Hsieh, D.-Y., and M. S. Plesset, Theory of rectified diffusion of mass into gas bubbles, *J. Acoust. Soc. Am.*, **33**, 206–215, 1961.
- Johnston, M. J. S., A. T. Linde, and D. C. Agnew, Continuous borehole strain in the San Andreas fault zone before, during, and after the 28 June 1992, M_w 7.3 Landers, California, earthquake, *Bull. Seismol. Soc. Am.*, **84**, 799–805, 1994.
- Johnston, M. J. S., D. P. Hill, A. T. Linde, J. Langbein, and R. Bilham, Transient deformation during triggered seismicity from the June 28, 1992, $M_w = 7.3$ Landers earthquake at Long Valley volcanic caldera, California, *Bull. Seismol. Soc. Am.*, in press, 1995.
- Julian, B. R., Evidence for dike intrusion earthquake mechanisms near Long Valley caldera, California, *Nature*, **303**, 323–325, 1983.
- Julian, B. R., and S. A. Sipkin, Earthquake processes in the Long

- Valley caldera area, California, *J. Geophys. Res.*, **90**, 11,155–11,169, 1985.
- Kanamori, H., H-K Thio, D. Dreger, and E. Hauksson, Initial investigation of the Landers, California, earthquake of 28 June 1992 using TERRASCOPE, *Geophys. Res. Lett.*, **19**, 2267–2270, 1992.
- King, G. C. P., R. S. Stein, and J. Lin, Static stress changes and the triggering of earthquakes, *Bull. Seismol. Soc. Am.*, **84**, 935–953, 1994.
- Kissling, E., Geotomography with local earthquake data, *Rev. Geophys.*, **26**, 659–698, 1988.
- Kisslinger, C., The stretched exponential function as an alternative model for aftershock decay rate, *J. Geophys. Res.*, **98**, 1913–1922, 1993.
- Kisslinger, C., and L. M. Jones, Properties of aftershock sequences in southern California, *J. Geophys. Res.*, **96**, 11,947–11,958, 1991.
- Knopoff, L., and M. J. Randall, The compensated linear-vector dipole: A possible mechanism for deep earthquakes, *J. Geophys. Res.*, **75**, 4957–4963, 1970.
- Lachenbruch, A. H., J. H. Sass, R. J. Munroe, and T. H. Moses Jr., Geothermal setting and simple heat conduction models for the Long Valley caldera, *J. Geophys. Res.*, **81**, 769–784, 1976.
- Langbein, J. O., Deformation of the Long Valley caldera, eastern California from mid-1983 to mid-1988: measurements using a two-color geodimeter, *J. Geophys. Res.*, **94**, 3833–3849, 1989.
- Langbein, J. O., D. Dzuris, G. Marshall, R. Stein, and J. Rundle, Shallow and peripheral volcanic sources of inflation revealed by modeling two-color geodimeter and leveling data from Long Valley caldera, 1988–1992, *J. Geophys. Res.*, in press, 1995.
- Langbein, J. O., D. P. Hill, T. N. Parker, and S. K. Wilkinson, An episode of reinflation of the Long Valley caldera, eastern California: 1989–1991, *J. Geophys. Res.*, **98**, 15,851–15,870, 1993.
- Lide, C. S., and A. S. Ryall, Aftershock distribution related to the controversy regarding mechanisms of the May 1980, Mammoth Lakes, California, earthquakes, *J. Geophys. Res.*, **90**, 11,151–11,155, 1985.
- Linde, A. T., I. S. Sacks, M. J. S. Johnston, and D. P. Hill, Long Valley triggered strain and seismicity: Can bubbles do it?, *Nature*, **371**, 408–410, 1994.
- Lockner, D., The role of acoustic emission in the study of rock fracture, I, *Int. J. Rock Mech. Min.*, **30**, 883–899, 1993.
- McHugh, S., and M. J. S. Johnston, An analysis of coseismic tilt changes from an array in central California, *J. Geophys. Res.*, **82**, 5692–5698, 1977.
- Michael, A., Initiation of seismicity remotely triggered by the Landers earthquake: Where and when, (abstract), *Eos Trans. AGU*, **73**(43), Fall Meeting suppl., 392–393, 1992.
- Mogi, K., Relations between eruptions of various volcanoes and the deformations of the ground surfaces around them, *Bull. Earthquake Res. Inst. Univ. Tokyo*, **36**, 99–134, 1957.
- Mogi, K., Study of elastic shocks caused by the fracture of heterogeneous materials and its relation to earthquake phenomena, *Bull. Earthquake Res. Inst. Univ. Tokyo*, **40**, 125–173, 1962.
- Moore, D. E., D. A. Lockner, and J. D. Byerlee, Reduction of permeability in granite at elevated temperatures, *Science*, **265**, 1558–1561, 1994.
- Moos, D., and M. D. Zoback, State of stress in the Long Valley caldera, California, *Geology*, **9**, 837–840, 1993.
- Mortensen, C. E., and D. G. Hopkins, Tiltmeter measurements in Long Valley caldera, California, *J. Geophys. Res.*, **92**, 13,767–13,776, 1987.
- Murase, T., and A. R. McBirney, Properties of some common igneous rocks and their melts at high temperatures, *Geol. Soc. Am. Bull.*, **84**, 3563–3592, 1973.
- Okada, Y., Surface deformation due to shear and tensile faults in a half-space, *Bull. Seismol. Soc. Am.*, **75**, 1135–1154, 1985.
- Okada, Y., Internal deformation due to shear and tensile faults in a half-space, *Bull. Seismol. Soc. Am.*, **82**, 1018–1040, 1992.
- Okada, Y., and E. Yamamoto, Dyke intrusion for the 1989 seismo-volcanic activity off Ito, central Japan, *J. Geophys. Res.*, **96**, 10,361–10,376, 1991.
- Pitt, A. M., and D. P. Hill, Long-period earthquakes in the Long Valley caldera region, eastern California, *Geophys. Res. Lett.*, **21**, 1679–1682, 1994.
- Ponko, S. C., and C. O. Sanders, Inversion for *P* and *S* wave attenuation structure, Long Valley caldera, California, *J. Geophys. Res.*, **99**, 2619–2635, 1994.
- Rice, J. R., and M. P. Cleary, Some basic stress diffusion solutions for fluid-saturated elastic porous media with compressible constituents, *Rev. Geophys.*, **14**, 227–241, 1976.
- Roeloffs, E. A., S. Schulz Burford, F. S. Riley, and A. W. Records, Hydrologic effects on water level changes associated with episodic fault creep near Parkfield, California, *J. Geophys. Res.*, **94**, 12,387–12,402, 1989.
- Roeloffs, E. A., W. R. Danskin, C. D. Farrar, D. L. Galloway, S. N. Hamlin, E. G. Quilty, M. L. Sorey, and D. E. Woodcock, Hydrologic effects associated with the June 28, 1992 Landers, California, earthquake sequence, *U.S. Geol. Surv. Open File Rep.*, **95-42**, 68 pp., 1995.
- Romero, A. E., Jr., T. V. McEvelly, E. L. Majer, and A. Micheline, Velocity structure of the Long Valley caldera from the inversion of local earthquake *P* and *S* travel times, *J. Geophys. Res.*, **98**, 18,869–18,879, 1993.
- Roquemore, G. R., and G. W. Simila, Aftershocks from the 28 June 1992 Landers earthquake: Northern Mojave Desert to the Coso Volcanic Field, California, *Bull. Seismol. Soc. Am.*, **84**, 863–891, 1994.
- Ruff, L., Some implications of the Landers case for remote triggering of seismicity (abstract), *Eos Trans. AGU*, **74**(43), Fall Meeting suppl., 448, 1993.
- Sahagian, D. L., and A. A. Proussevitch, Advective bubble overpressure in volcanic systems, *Nature*, **359**, 485, 1992.
- Sanders, C. O., Reanalysis of *S*-to-*P* amplitude ratios for gross attenuation structure, Long Valley caldera, California, *J. Geophys. Res.*, **98**, 22,069–22,076, 1993.
- Savage, J. C., and R. S. Cockerham, Earthquake swarm in Long Valley caldera, California, January 1983: Evidence for dike injection, *J. Geophys. Res.*, **89**, 8315–8324, 1983.
- Sieh, K., et al., Near-field investigations of the Landers earthquake sequence, April to July 1992, *Science*, **260**, 171–176, 1993.
- Sorey, M. L., B. M. Kennedy, W. C. Evans, C. D. Farrar, and G. A. Suemnicht, Helium isotope and gas discharge variations associated with crustal unrest in Long Valley caldera, California, *J. Geophys. Res.*, **98**, 15,871–15,889, 1993.
- Spudich, P., L. K. Steck, M. Hellweg, J. B. Fletcher, and L. M. Baker, Transient stresses at Parkfield, California, produced by the *M* 7.4 Landers earthquake of June 28, 1992: Observations from the UPSAR dense seismograph array, *J. Geophys. Res.*, **100**, 675–690, 1995.
- Steck, L. K., and W. A. Prothero Jr., Crustal structure beneath Long Valley caldera from modeling of teleseismic *P* wave polarizations and *P_s* converted waves, *J. Geophys. Res.*, **99**, 6881–6898, 1994.
- Stein, R. S., G. C. P. King, and J. Lin, Change in failure stress on the southern San Andreas fault system caused by the 1992 magnitude = 7.4 Landers earthquake, *Science*, **258**, 1328–1332, 1992.
- Talwani, P., and S. Acree, Pore pressure diffusion and the mechanism of reservoir-induced seismicity, *Pure Appl. Geophys.*, **122**, 946–965, 1984/85.
- Wilshire, H. G., and S. H. Kirby, Dikes, joints, and faults in the upper mantle, *Tectonophysics*, **161**, 23–31, 1989.
- Wyatt, F. K., D. C. Agnew, and M. Gladwin, Continuous measurements of crustal deformation for the 1992 Landers earthquake sequence, *Bull. Seismol. Soc. Am.*, **84**, 768–779, 1994.
- Zoback, M. D., and M. L. Zoback, Tectonic stress field of North America and relative plate motions, in *The Geology of North America*, Decade Map Vol. 1, *Neotectonics of North America*, edited by D. B. Slemmons, E. R. Engdahl, M. D. Zoback, and D. D. Blackwell, pp. 339–366, Geological Society of America, Boulder, Colo., 1991.

R. Bilham, Department of Geology, University of Colorado, Boulder, CO 80309. (e-mail: bilham@spot.colorado.edu)

D. P. Hill, M. J. S. Johnston, and J. O. Langbein, U.S. Geological Survey, MS977, 345 Middlefield Road, Menlo Park, CA 94025. (e-mail: hill@andreas.wr.usgs.gov; mal@thebeach.wr.usgs.gov; langbein@thebeach.wr.usgs.gov)

(Received March 18, 1994; revised March 3, 1995; accepted March 13, 1995.)